ASSESSMENT OF INDOOR RADON CONCENTRATION LEVELS IN SERULE, BOTSWANA

by

Refilwe Setso

Student Reg. No: **17100133**

BSc (Radiation and Health Physics, UoB)

Department of Physics and Astronomy,

Faculty of Sciences,

Botswana International University of Science and Technology

setso.refilwe@studentmail.biust.ac.bw, (+267) 75990133

A Dissertation Submitted to the Faculty of Sciences in Fulfilment of the Requirements for the Award of the Master of Science in Physics of BIUST

Supervisor:

Dr. Chamunorwa Oscar Kureba

Department of Physics and Astronomy,

Faculty of Sciences, BIUST

kurebac@biust.ac.bw, (+267) 493 1558

Signature:_____ Date:04/08/2020

Co-supervisor:

Dr. Peane P. Maleka

Department of Subatomic Physics

iThemba LABS

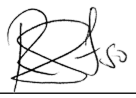
pmaleka@tlabs.ac.za, +27 218 431 025

Signature:_____ Date:04/08/2020

04 August 2020

Declaration and Copyright

I, **Refilwe Setso**, declare that this dissertation is my own original work and that it has not been, and will not be presented to any other university for a similar or any other degree award.

Signature:  Date: 04/08/2020

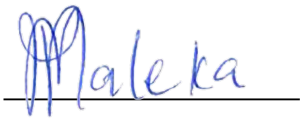
This dissertation is copyright material protected under the Berne Convention, the Copyright Act of 1999 and other international and national enactments, in that behalf, on intellectual property. It must not be reproduced by any means, in full or in part, except for short extracts in fair dealing; for researcher private study, critical scholarly review or discourse with an acknowledgement, without the written permission of the office of the Provost, on behalf of both the author and the BIUST.

Certification

The undersigned certify that they have read and hereby recommends for acceptance by the Faculty of Sciences a dissertation titled: **Assessment of Indoor Radon Concentration Levels in Serule, Botswana**, in fulfilment of the requirements for the degree of Master of Science (MSc Physics) of the Botswana International University of Science and Technology.



Dr. Chamunorwa Oscar Kureba
(Supervisor)
Date: 04/08/2020



Dr. Peane Peter Maleka
(Co-Supervisor)
Date: 04/08/2020

Acknowledgements

I want to appreciate the following people and institutions for the role that they played in making this thesis possible:

Dr. Chamunorwa O. Kureba, supervisor, for the mentor-ship, support, invaluable advice and for always going an extra mile to make sure finances are readily available to facilitate my study needs.

A special thank you to the **Physics and Astronomy Department**, my fellow post-graduate students, especially those from the Applied Nuclear and Radiation Physics group for their support and encouragement, **Babedi Sebinanyane** who has been there on almost all my Serule field trips to offer a helping hand.

Dr. Peane P. Maleka, co-supervisor, for his guidance and full support. Many thanks to **iThemba LABS** for providing me with the necessary equipment for my work. I would also like to thank Dr. Maleka's students at the Environmental Radioactivity Laboratory at iThemba LABS for providing me with technical assistance, **Avuyile Bulala** and **Mistura Ajani**.

The Serule residents who were so willing and permitted me to set-up equipment and take measurements in their homes. My parents, family and friends who have all stood by me and been my source of encouragement throughout. And last but not least, I want to thank God for enabling me to come this far.

Dedication

To my loving parents, Mr. Goboletswe Setso and Mrs. Karabo Setso who have been there for me since I began my studies, they have truly been an inspiration and my backbone in this academic journey.

Abstract

Discoveries of huge uranium deposits along the Letlhakane and Serule area in Botswana, led and motivated various researchers to investigate the long term effects of these discoveries. In addition to economic benefits, the possibility of environmental pollution is also high. This study assesses the indoor radon concentration levels in Serule area. Radon (^{222}Rn) is of interest because, it is a daughter radionuclide of Radium-226 (^{226}Ra) from the Uranium-238 (^{238}U) decay series and can cause adverse health problems such as lung cancer when inhaled. It is odourless, tasteless, colourless and there is no way of knowing how much of it you are exposed to unless you measure it.

The indoor radon concentration levels were measured in 10 houses in Serule using passive radon monitors called the E-PERMS (Electret-Passive Environmental Radon Monitors) and 2 houses in Palapye were used as the control. Of the 10 houses in Serule, 6 houses were within the proposed mining area and 4 outside the mining area. The weighted average indoor radon concentration in Serule area from the sampled houses, was found to be 23.4 $\pm$ 2.1 Bq/m^3 and from the control houses it was 7.0 $\pm$ 0.3 Bq/m^3. The results obtained are below the recommended limit of 300 Bq/m^3 as per the IAEA regulations. It was also observed that, the highest radon concentration levels were recorded in the summer and winter seasons. The building materials used in the construction of the sampled houses along with the ventilation habits of the inhabitants also influenced the amount of radon concentrations recorded. The main contributor however, was the uranium rich underlying rocks as the radon concentration was higher in areas within the mining area than those

outside. The average annual effective dose received by the Serule residents in the sampled houses from inhalation of radon was calculated to be 0.67 ± 0.23 mSv and only 0.1764 ± 0.0071 mSv was received in the control houses. The obtained results are below the 3 - 10 mSv dose limit recommended by the ICRP.

Soil samples from the vicinity of the sampled houses were collected and counted using a High Purity Germanium (HPGe) detector at iThemba LABS. Gamma spectrometry was used in this case to obtain the activity concentration of each radionuclide contained in a given sample. The activity concentrations of ^{238}U, ^{232}Th and ^{40}K obtained ranged from 6 - 658 Bq.kg^{-1}. The highest activity concentration of ^{238}U was found in areas within the mining area, and the activity concentration of ^{232}Th was generally low across all areas sampled. The activity concentration of ^{40}K showed high levels in sampled areas outside the mining area and this might be related to potassium rich fertilizers used for agricultural productions in their homes. The radiological hazard assessment indicated that the highest radium equivalent (Ra_{eq}) value calculated was 164.1 ± 12.2 Bq.kg^{-1} from SSH3 which was within the mining area. The results for all other Ra_{eq} values obtained in this study are below the 370 Bq.kg^{-1} limit set by IAEA. Two sampled locations within the mining area (SH3 and SH4) had the highest absorbed dose rate of 75.0 ± 12.5 nGy.h^{-1} and 69.6 ± 10.4 nGy.h^{-1} respectively, which were higher than world average value of 57 nGy.h^{-1}. The calculated external and internal hazard indices of all the twelve soil samples were below 1, with the highest value being 0.7 meaning the risk due to exposure is generally low. The heavy metals concentration in the soil samples were determined using Inductively Coupled Plasma-Mass Spectrometry (ICP-MS). Only nine of the heavy metals were of interest, that is, chromium, nickel, arsenic, copper, zinc, cobalt, lead, mercury and cadmium. Soil sample SSH7 had the highest concentration of heavy metals, with the nickel and cadmium concentrations being higher than the maximum allowable limit according to WHO/FAO guidelines of 50 mg/kg and 100 mg/kg with values of 109.282 mg/kg and 158.213 mg/kg respectively. Soil samples collected in Serule had slightly higher heavy metals concentration compared to those from the control area.

Contents

Declaration ii

Certification iii

Acknowledgements iv

Dedication v

Abstract vi

List of Figures xii

List of Tables xvi

List of Abbreviations xvii

1 Introduction 1

1.1 Historical background 1

1.2 Problem definition 3

1.3 Project Aim 4

1.3.1 Specific Objective 4

1.3.2 Key questions 4

1.4 Justification of the study 5

1.5 Dissertation outline 5

2 Background Literature **6**

2.1 Radioactivity . . . 6

2.2 The Radioactive Decay Law . . . 7

2.2.1 Alpha Decay . . . 8

2.2.2 Beta Decay . . . 9

2.2.3 Gamma Decay . . . 10

2.3 Properties of radon . . . 10

2.4 Isotopes of radon . . . 11

2.5 ^{238}U Decay series . . . 11

2.6 ^{232}Th Decay series . . . 12

2.7 The ^{235}U Decay series . . . 13

2.8 Emanation and exhalation of radon gas . . . 14

2.8.1 Radon Emanation Coefficient . . . 15

2.8.2 Radium distribution, soil moisture, porosity and grain size . . . 16

2.9 Radon entry into a house . . . 17

2.9.1 Factors influencing radon concentration levels indoors . . . 18

2.10 Risks of exposure to radon . . . 18

2.11 Dose quantities and Calculations . . . 19

2.12 Available literature . . . 22

3 Experimental Methods and Data Analysis **24**

3.1 Introduction . . . 24

3.2 Description of the Study Area . . . 24

3.2.1 The Area of Interest . . . 25

3.2.2 Materials used for the construction of the houses . . . 26

3.3 Principles of Radon Detection Systems . . . 28

3.3.1 The E-PERM system . . . 29

3.3.2 Operation of the Electret . . . 30

3.3.3 The E-PERM Electret Ion Chamber . . . 30

3.3.4 Electret Voltage Readers . . . 33

3.4 Measurement of radon concentration levels using E-PERMS 34
3.5 Soil sample collection and preparation 36
3.6 Analytical techniques used on the soil samples 40
3.6.1 The High Purity Germanium (HPGe) detector 40
3.6.1.1 Energy calibration for Gamma Spectrometry 42
3.6.1.2 Energy calibration curve 43
3.6.1.3 Full energy peak efficiency calibration 43
3.6.2 Calculation of activity concentrations 45
3.6.3 Radiological hazard effects 47
3.6.3.1 Radium Equivalent Activity 47
3.6.3.2 Absorbed dose rate 47
3.6.3.3 Hazard indices 48
3.6.4 The Inductively Coupled Plasma Mass Spectrometry (ICP-MS) . . 48

4 Results and Interpretation 50

4.1 Introduction 50
4.2 Average Indoor Radon Concentration 50
4.2.1 Monthly variations of radon concentration levels 52
4.2.2 Seasonal Variations 58
4.2.3 Influence of house design on the radon concentration 60
4.3 Annual effective dose from inhalation of radon 60
4.4 Activity concentrations of ^{238}U, ^{232}Th and ^{40}K in the soil samples 61
4.4.1 Radiological hazard assessment for soil samples 65
4.5 Concentration of Heavy metals in soil samples 66

5 Conclusions and Recommendations 69

5.1 Introduction 69
5.2 Summary and conclusions 69
5.3 Recommendations 72

Appendix A Sampled houses dimensions 73

Appendix B Parameters for radon concentration calculation 74

Appendix C Activity Concentration of observed radionuclides 78

Appendix D ICP-MS results from the Central Analytical Facilities (CAF) 80

References 82

List of Figures

1.1 The global contribution of natural sources to the average annual effective dose, total of 2.4 mSv 2

2.1 Ionization process due to radiation 7
2.2 Alpha decay process 8
2.3 Beta-minus decay process 9
2.4 Gamma decay process. 10
2.5 Decay series of ^{238}U 12
2.6 Decay series of ^{232}Th 13
2.7 Decay series of ^{235}U 14
2.8 Radon emanation, migration and exhalation into the atmosphere 15
2.9 Schematic diagram of how radon emanates from soil grain 16
2.10 Radon pathways into a house 18
2.11 Health risk of exposure to radon gas. 19

3.1 A-Cap Resources Uranium mining licensed area demarcations in Serule . . 25
3.2 Sampling points (white circles) of the selected Serule homes used for the study as obtained from the GPS, SH9 and SH10 are in close proximity. . . 26
3.3 Examples of some of the selected Serule houses, where radon measurements were conducted. 27
3.4 The Electret Passive Environmental Radon Monitor system. 29

3.5 Electrets manufactured by Rad Elec Inc. 30
3.6 Chambers manufactured by Rad Elec Inc. 31
3.7 The E-PERM S-chamber in a closed position during storage or when not in use and during radon measurement when in an open position. 32
3.8 The mechanism of radon entry into the E-PERM S-chamber. 32
3.9 Figure (a) shows SPER-1 voltage reader and Figure (b) shows SPER-2 Voltage reader. 33
3.10 Typical example of how the E-PERM chambers were mounted in a house. . 34
3.11 The Garmin GPS device used in the current study. 37
3.12 Soil sample collection using an auger 37
3.13 Steps of soil preparation. 39
3.14 Schematic diagram of the HPGe system at iThemba LABS. 41
3.15 Energy calibration curve showing the relation of channels and energy. . . . 43
3.16 The efficiency curve of the ERL HPGe detector as a function of energy, showing the fit parameters from the ^{238}U and ^{40}K data points. 45
3.17 A spectrum of observed radionuclides from one of the soil samples used in the current study. 46
3.18 The ICP-MS system used in analysing the soil samples. 49

4.1 Average indoor radon concentration in the selected dwellings. 51
4.2 Distribution of indoor radon concentration levels in SH1 across the months relative to the average indoor radon concentration level. 52
4.3 Distribution of indoor radon concentration levels in SH2 across the months relative to the average indoor radon concentration level. 53
4.4 Distribution of indoor radon concentration levels in SH3 across the months relative to the average indoor radon concentration level. 53
4.5 Distribution of indoor radon concentration levels in SH4 across the months relative to the average indoor radon concentration level. 54
4.6 Distribution of indoor radon concentration levels in SH5 across the months relative to the average indoor radon concentration level. 54

4.7 Distribution of indoor radon concentration levels in SH6 across the months relative to the average indoor radon concentration level. 55
4.8 Distribution of indoor radon concentration levels in SH7 across the months relative to the average indoor radon concentration level. 55
4.9 The distribution of indoor radon concentration levels in SH8 across the months relative to the average indoor radon concentration level. 56
4.10 The distribution of indoor radon concentration levels in SH9 across the months relative to the average indoor radon concentration level. 56
4.11 The distribution of indoor radon concentration levels in SH10 across the months relative to the average indoor radon concentration level. 57
4.12 The distribution of indoor radon concentration levels in PH1 across the months relative to the average indoor radon concentration level. 57
4.13 Distribution of indoor radon concentration levels in PH2 across the months relative to the average indoor radon concentration level. 58
4.14 Seasonal variations of the radon concentration in the selected dwellings. . . 59
4.15 The ^{226}Ra activity concentration levels in the selected sampled locations. . 63
4.16 The ^{232}Th activity concentration levels in the selected sampled locations. . 64
4.17 The ^{40}K activity concentration levels in the selected sampled locations. . . 64
4.18 The Radium equivalent (Ra_{eq}) values for each soil sample. 65
4.19 The ratio of heavy metals in selected soil samples with respect to WHO/-FAO guidelines. 68

List of Tables

2.1 Physical properties of radon gas 11
2.2 Projected range of radon atoms in different mediums. 17
2.3 Types of radiation and their respective radiation weighting factors 20
2.4 Different organs and their tissue weighting factors 21
2.5 Residential radon concentration levels in some countries in the OECD . . . 22

3.1 The building materials used in the construction of selected houses 27
3.2 Soil sample codes and their respective GPS coordinates. 38
3.3 Soil sample codes and their respective mass in kilograms. 40
3.4 Gamma-ray lines from ^{232}Th used for energy calibration 42
3.5 MCA channel numbers and their corresponding gamma-ray peaks from ^{232}Th. 43
3.6 Gamma-ray lines from ^{238}U used for efficiency calibration 44
3.7 Gamma-ray line from ^{40}K used for efficiency calibration 45

4.1 The average indoor radon concentration levels in the twelve selected houses. 51
4.2 The annual effective dose in the 12 sample houses. 61
4.3 The activity concentrations of ^{226}Ra, ^{232}Th and ^{40}K. 62
4.4 The calculated results of absorbed dose (D), radium equivalent (Ra_{eq}), external hazard index (H_{ex}) and internal hazard index (H_{in}). 66
4.5 The concentration of Heavy metals in the selected soil samples in mg/kg. . 67

A.1 The dimensions of the rooms used in the current study, where the E-PERMS were deployed 73

B.1 The average indoor radon concentration level in each dwelling in various seasons 77

C.1 The activity concentrations of observed ^{238}U daughter radionuclides. 79

C.2 The activity concentrations of observed ^{232}Th daughter radionuclides. 79

List of Abbreviations

- **NORM** Naturally Occurring Radioactive Materials
- **ICRP** International Committee on Radiation Protection
- **IAEA** International Atomic Energy Agency
- **WHO** World Health Organization
- **FAO** Food and Agriculture Organization
- **iThemba LABS** iThemba Laboratory for Accelerator Based Sciences
- **E-PERM** Electret Passive Environmental Radon Monitors
- **ICP-MS** Inductively Coupled Plasma-Mass Spectrometry
- $\mathbf{Ra}_{eq}$ Radium Equivalent
- $\mathbf{H}_{ex}$ External hazard index
- $\mathbf{H}_{in}$ Internal hazard index
- **BDL** Below Detection Limit
- **DCF** Dose Conversion Factor

1

Introduction

1.1 Historical background

Radon (^{222}Rn) is a naturally occurring tasteless, odourless and colourless radioactive gas from the natural decay of uranium ^{238}U. Radon has three main isotopes, that is, ^{222}Rn, ^{220}Rn (thoron) and ^{219}Rn (actinon). Radon for this study will refer to ^{222}Rn which has a half-life of about 3.824 days. Radon was first acknowledged by Friedrich Ernst Dorn in 1900, who referred to it as radium emanation. This is because, it is the immediate decay product of Radium-226 (^{226}Ra) in the decay series of Uranium-238 (^{238}U), an element found in most rock and soil types [1].

Natural radiation in the environment generally occurs at levels that are not hazardous to human health. The health risk usually comes into play when the natural radiation concentration are enhanced by anthropogenic activities such as mining [2]. These elevated radiation levels found in the environment are referred to as Naturally Occurring Radioactive Materials (NORMs). There are three main categories of radionuclides available in the environment, namely, terrestrial, cosmogenic and anthropogenic radionuclides. Terrestrial radionuclides, which are sometimes referred to as primordial radionuclides originate from rocks of the earth, from food and drinks. These radionuclides often have half lives in the order of a billion years and examples of such include ^{40}K, ^{235}U and ^{238}U. Cosmogenic

radionuclides are a result of the interaction of cosmic rays with the earth's atmosphere. Examples of such radionuclides include ^{14}C and ^{14}Na. Anthropogenic radionuclides on the other hand, are due to man-made activities, for example ^{137}Cs which is a result of nuclear fission in fuel rods in nuclear power plants [3].

Radon is by far the largest naturally occurring source of ionizing radiation in the environment [4]. Radon and its daughter products or progeny (Polonium-218 and Polonium-214) are estimated to contribute 50 % of the annual effective dose received by human beings [5] , as illustrated in Figure 1.1. Technologically Enhanced Naturally Occuring Radioactive Materials (TENORM) are found in the environment and are by-products of enriched radioactive elements or industrial waste. These elements include uranium, thorium, potassium and any of their daughter products, such as radium and radon [6]. TENORMs therefore, also contribute to the amount of radon found in a particular area.

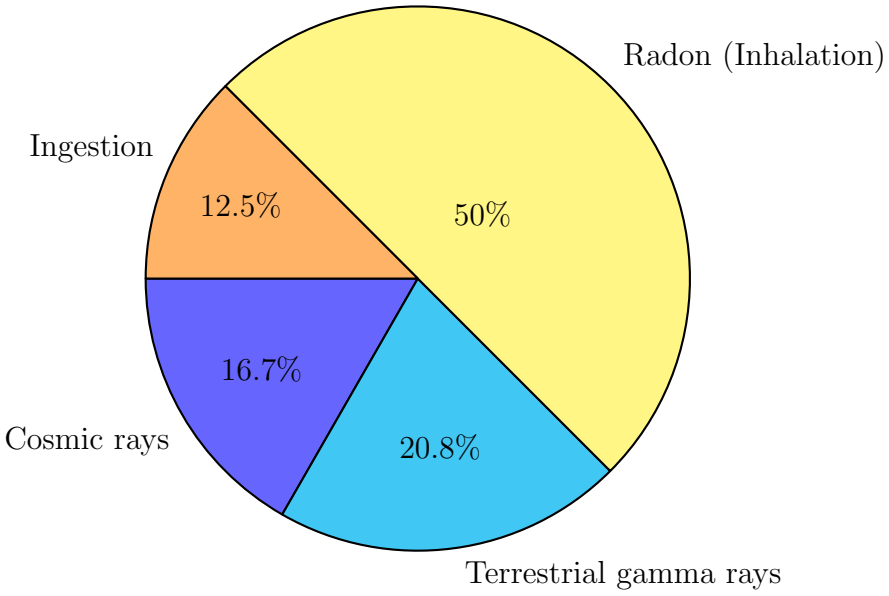


Figure 1.1: The global contribution of natural sources to the average annual effective dose, total of 2.4 mSv [5].

1.2 Problem definition

Radon decays by emitting alpha radiation and when inhaled it can damage tissues in the respiratory tract, thereby increasing the risk of lung cancer [7]. For the past decades, the scientific community has been interested in finding out the chances of cancer induction due to indoor radon and the United States of America's Environmental Protection Agency (EPA) acknowledge radon as the second leading cause of lung cancer after tobacco smoking [8]. Depending on the country, acceptable residential radon levels vary but a generally accepted reference level is set at 300 Bq/m^3 based on the International Committee on Radiation Protection (ICRP) recommendations [9]. The International Atomic Energy Agency (IAEA) also recommends that the national reference level be less or equal to 300 Bq/m^3 [4].

A search through the available literature, found no documentation that provides any radon reference levels for Botswana as a country. With the discovery of huge uranium deposits in Botswana along the Letlhakane and Serule area and considering that radon is one of the daughter nuclei in the decay series of uranium, there is a possibility of levels being enhanced as compared to other areas in the country [10]. There are currently ongoing studies on the radiological risk assessment of surface and ground water sources in Serule area and some studies on the radiometric analysis of Serule soils by BIUST researchers. However, there has not been any study carried out in that area, on the radiological effects of the discovered uranium deposits on air, so as to give a complete overview of the effects of radioactivity on the Serule environment (soil, water and air). One important aspect of Radiation Protection is to protect the public from ionising radiation and as such, it is important to study and record the levels of indoor radon in these mining areas before the actual mining commence.

1.3 Project Aim

The aim of the study was to make a qualitative and quantitative analysis of the average indoor radon concentration in residential houses in Serule, Botswana.

This study sought to determine the average indoor radon concentration levels in selected homes in the Serule area of Botswana, where uranium mining is due to commence. Estimation of the annual effective dose received by residents of Serule will be reported. The study will further determine the seasonal variations of radiation exposure by measuring the radon levels during summer, autumn and winter seasons.

1.3.1 Specific Objective

- To determine the influence of seasonal variations and building materials on the concentration of indoor radon.
- To calculate the annual effective dose received by residents of Serule due to radon exposure,
- To determine the activity concentration of various radionuclides found in the soil samples of selected areas and carry out a radiological hazard assessment.
- To determine the concentration of heavy metals in some selected soil samples from the sampled areas.

1.3.2 Key questions

- Are there any ventilation systems put in place to minimise the accumulation of indoor radon levels in the houses?
- Which type and origin of building materials were used in the construction of the houses?

1.4 Justification of the study

The outcome of the study is expected to provide a baseline for the indoor radon concentration level in Serule before mining starts. This study should be seen as a pilot investigation that possibly lead to follow-up investigations especially after mining starts, to identify the effects of anthropogenic activities. The study is also important in raising awareness to the population living around uranium mining areas about the potential health risks raised by radioactivity.

1.5 Dissertation outline

The arrangement of the dissertation is as follows;

- Chapters 1 presents the background theory on radon and introduces the problem statement and the aims and objectives of the study.
- Chapter 2 gives a general description of radioactivity, radon gas and its emanation, risks of exposure to radon, dose calculations and also the literature review from other similar studies.
- Chapter 3 presents the relevant measuring techniques and methods used to collect and measure all the study data.
- Chapter 4 presents the results of the study and the interpretation and discussion of the results.
- Chapter 5 presents the conclusion and recommendations of the study.

2

Background Literature

In this chapter we look at the background theory associated with radiation in general, radon properties and its emanation and entry points into a house. The risks of human health and the dose associated with exposure to radon. This chapter also looks at similar studies that have been carried out on indoor radon concentration levels in houses.

2.1 Radioactivity

In 1896, a French physicist Henri Becquerel discovered radioactivity and since then, many studies have been carried out on the science of radioactivity [11]. Radioactivity is the natural and spontaneous disintegration of unstable atomic nuclei into more stable daughter nuclei without the effect of chemical and physical conditions [12]. During the disintegration process, energy is released by the emission of nuclear particles such as alpha particles, beta particles and gamma rays.

X-rays, positrons and neutrons may also be emitted during a radioactive decay. All these emissions are called ionizing radiations and it is the ionizing nature of these emissions that makes them a hazard to health. Ionizing radiation arise from both natural and also man-made radionuclides. Ionization is a process in which an atom acquires a positive or a negative charge by losing or gaining electrons thereby becoming an ion which is

an electrically charged atom. Figure 2.1 depicts the process of ionization as a result of radiation interacting with an atom. The electron gets knocked off by the radiation.

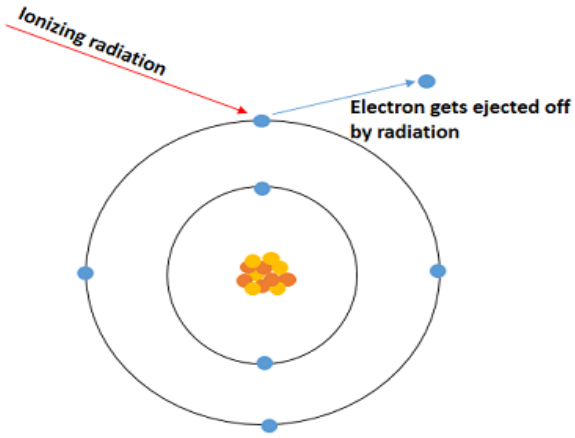


Figure 2.1: Ionization process due to radiation

2.2 The Radioactive Decay Law

The decay process of radioactive nuclides is statistical and prediction of when a certain atom would decay to form another is quite impossible. However, the decay will follow a well-defined statistical pattern if a large number of atoms are looked at as a single unit. This statistical pattern is known as the radioactive decay law [13]. The decay (dN) of a radioactive nucleus at a certain time (dt) would be proportional to the total number of nuclei N given that there isn't any formation of new nuclei in that sample. This is mathematically represented in equation 2.1.

$$\frac{dN}{dt} = -\lambda N, \tag{2.1}$$

where λ (s^{-1}) is the decay constant, that is, the probability for the decay of an atom per unit time. The value of λ is unique for each nuclide and it is related to the half-life ($t_{1/2}$) of a radionuclide. Half-life is the time required for a radioactive nuclide to decay to half of the original number of nuclei present [13]. Half-life is given by equation 2.2:

$$\frac{ln2}{\lambda} = t_{1/2} \tag{2.2}$$

Activity (A) is the number of disintegrations per unit time of a radioactive material. The activity of a number of radioactive atoms (N) is Nλ and the unit of activity is Becquerel (Bq), named after Henri Becquerel. One Becquerel is equivalent to one transformation/decay per second. The activity concentration is related to mass for solids and has units (Bq/kg), for liquids or gases the activity concentration is usually related to volume and has units (Bq/l or Bq/m^3) [14].

2.2.1 Alpha Decay

Decay by alpha emission is a natural process in heavy nuclei in the radioactive series. The parent atom emits an alpha particle, which is a helium atom, that is, it has two protons and two neutrons, making it very stable, see Fig. 2.2 and Eq. 2.3.

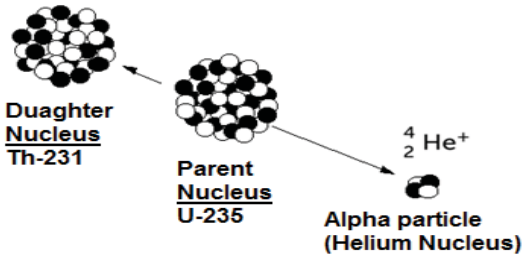


Figure 2.2: Alpha decay process

$$^{235}U \rightarrow ^{231}Th + ^{4}He \tag{2.3}$$

These electrically charged helium atoms can be ejected at relatively high speeds approximately 30 000 km/s (about 10% the speed of light) from the atom but slowed down and stopped by a sheet of paper of a thickness of about 0.05 mm or by 30 mm of air [15] . Although alpha particles cannot penetrate through the outer layer of skin, they make

a dense ionization trail along their stopping track. This can cause damage to biological tissue if emitted inside the body following ingestion or inhalation.

2.2.2 Beta Decay

Beta decay is of two types, that is, beta-minus (β^-) and beta-plus (β^+) decay. Beta-minus (see Eq. 2.4) is a radioactive process which emits an electron along with an antineutrino ($^0_0\nu$). In this decay process a neutron is converted into a proton resulting in an escape of an electron. A daughter atom is formed with one less neutron since the number of protons in the nucleus have changed [16]. A nucleus can also reach stability through the emission of a positively charged particle called a positron. The process is called beta-plus decay (see Eq. 2.5) and it is the exact opposite of what happens in a beta-minus decay. In this case, a proton decays into a positron and a neutron, while also emitting a neutrino (ν) as depicted in Fig. 2.3.

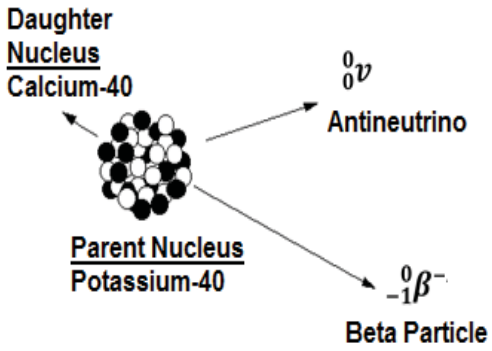


Figure 2.3: Beta-minus decay process

Beta-minus decay reaction:

$$n \rightarrow p^+ + e^- + {}^0_0\,\nu \tag{2.4}$$

Beta-plus decay reaction:

$$p^+ \rightarrow n + e^+ + \nu \tag{2.5}$$

2.2.3 Gamma Decay

Alpha and beta decay result in a nucleus that has more energy than usual and this excess energy is lost by the emission of gamma rays as illustrated in Fig. 2.4 [15]. Gamma rays are more penetrating than both alpha and beta particles and can only be stopped by high density materials such as lead.

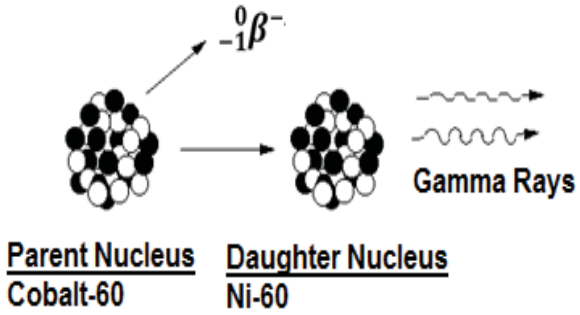


Figure 2.4: Gamma decay process.

2.3 Properties of radon

Radon is a group 8 element in the periodic table of elements, with an atomic number of 86 and a mass number of 222 a.m.u. It is the heaviest member of the inert gases. Because radon is an inert gas, it is generally not affected by chemical processes. It is soluble in water, which is capable of transporting it over long distances through the soil to the surface/atmosphere. It is colourless, odourless and tasteless making it undetectable by human senses. Special equipment have been designed specifically for the detection and measurement of radon gas in the environment. More details on the physical properties of radon are given in Table 2.1.

Table 2.1: Physical properties of radon gas

Boiling point at 1 atm pressure	-62° C
Density at 1 atm pressure and 0°C	9.73 g L^{-1}
Diffusion coefficient in water	10^{-5} cm^2s^{-1}
Diffusion coefficient in air	0.1 cm^2s^{-1}
Solubility in water at 1 atm pressure and 20°C	230 cm^3kg^{-1}
Viscosity at 1 atm pressure and 20°C	0.229 poise

2.4 Isotopes of radon

Radon has three natural isotopes, namely, ^{222}Rn, which has a half-life of $\sim$ 3.82 days, ^{220}Rn (thoron) with a half-life of $\sim$ 56 seconds and ^{219}Rn (actinon) which has a half-life of $\sim$ 3.96 seconds [17]. These isotopes are a result of the decay of some heavy elements, see the decay series of ^{238}U, ^{232}Th and ^{235}U in Figs. 2.5, 2.6 and 2.7.

2.5 ^{238}U Decay series

Radon (referring to Rn-222) is a daughter nucleus in the decay series of ^{238}U, see Figure 2.5, for the decay chain. ^{238}U undergoes a series of 14 decays to reach a stable nucleus, that is ^{206}Pb. Radon decays into radionuclides with relatively short half-lives and are chemically active. These radon daughter products can attach to airborne particles and be attached to respiratory tracts when inhaled by human beings and animals. The radon daughter products, that is, ^{218}Po and ^{214}Po are the most significant contributors to the lung dose via alpha emission, with alpha energies of about 6.00 and 7.69 MeV respectively [18].

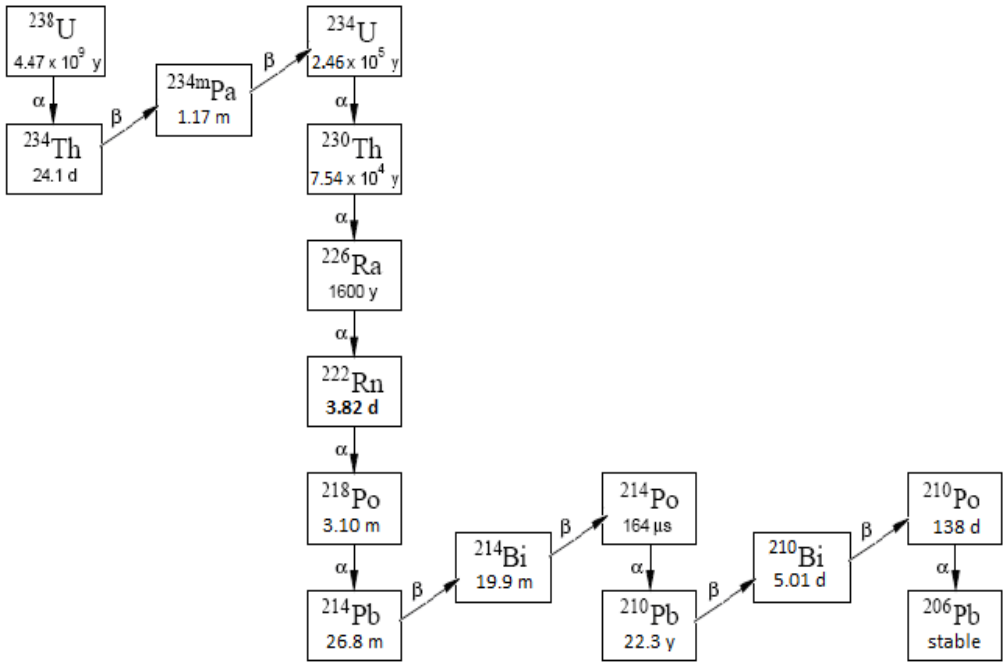


Figure 2.5: Decay series of ^{238}U [19].

2.6 ^{232}Th Decay series

In the decay chain of Th-232 shown in Fig. 2.6, thoron (^{220}Rn) is the most significant radionuclide followed by ^{212}Pb and ^{212}Bi with their contribution to the airborne concentrations. Since the daughter products of ^{220}Rn have slightly longer half-lives, their retention in the lung has some serious irradiation contribution through alpha decay. ^{212}Bi and ^{212}Po have alpha energies of 6.05 MeV and 8.78 MeV respectively and hence give rise to health implications [18].

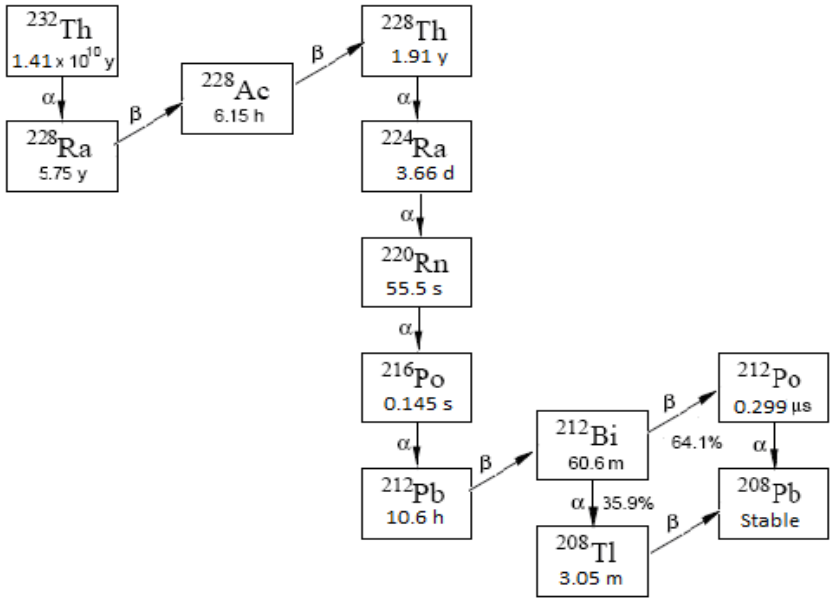


Figure 2.6: Decay series of ^{232}Th [19].

2.7 The ^{235}U Decay series

Actinon (^{219}Rn) is found in the decay series of ^{235}U and has a relatively shorter half-life as compared to its daughter products, ^{211}Pb and ^{211}Bi, see Fig. 2.7. Because ^{219}Rn decays and reaches its stable form quickly, it is not of much concern as compared to other isotopes ^{222}Rn and ^{220}Rn [18].

Since thoron (^{220}Rn) and actinon (^{219}Rn) have such short half-lives compared to radon (^{222}Rn), their penetration from the ground into a house, emanation from the building materials and also their movement are restricted to a few centimetres only. Radon (^{222}Rn) is therefore more of a concern compared to the other two isotopes.

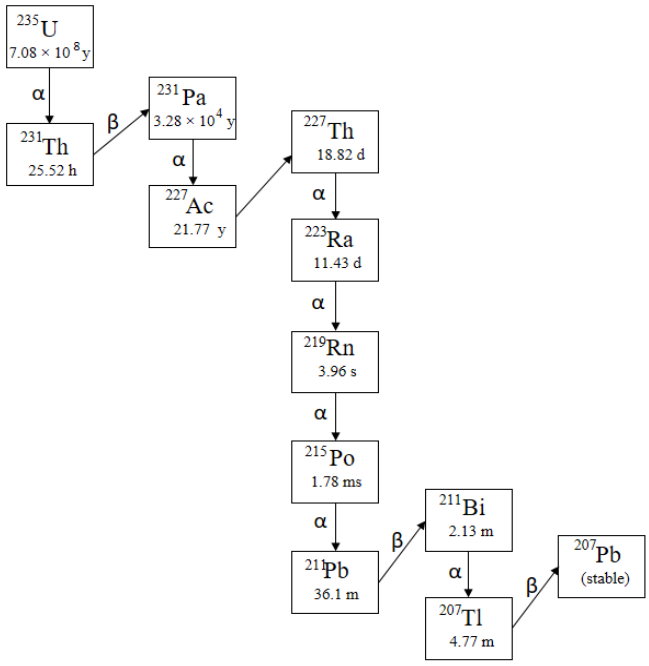


Figure 2.7: Decay series of ^{235}U [19].

2.8 Emanation and exhalation of radon gas

When the ^{226}Ra nucleus decays, it emits an alpha particle which causes a direct recoil resulting in radon emanation. Radon is released from a residue repository in a series of three processes as depicted in Fig. 2.8 namely [20];

- **Emanation:** When radium (^{226}Ra) decays, radon atoms get released from the soil grains into the interstitial space between those grains.
- **Transport:** The emanated radon atoms move through the soil pores and rock fractures from deep in the earth's crust to the ground surface by diffusion and advection.

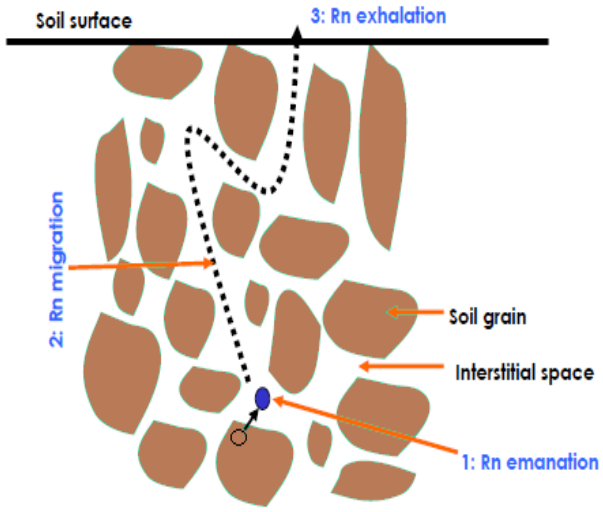


Figure 2.8: Radon emanation, migration and exhalation into the atmosphere [21].

- **Exhalation:** The radon atoms exhaled from the earth's surface into the atmosphere rapidly get diluted and dispersed by natural turbulence and convection. When there is a dwelling present, radon may move into the structure and accumulate indoors in significant quantities which may pose a hazard to health. This is illustrated in Fig. 2.8.

2.8.1 Radon Emanation Coefficient

The fraction of radon atoms that escapes from a medium into the interstitial space is known as the emanating power or emanation coefficient. Radon emanation coefficient is associated with the material, that is, soil, rocks, building materials or anything that contains radium. This is because, the radon emanation coefficient gives an indication of the fraction of the produced radon atoms that are released from the material [22].

When radium decays, its daughter radon escapes from a grain due to its recoil. The recoil in solids is relatively small, about 0.05 µm thus most of the recoiling atoms remain in the mineral grain lattice instead of being ejected out. In the event that the recoil occurs in an open pore or outside the grain, radon is able to migrate, see Figure 2.9 [19]. Table 2.2 further emphasizes the projected recoil range of radon atoms in different mediums.

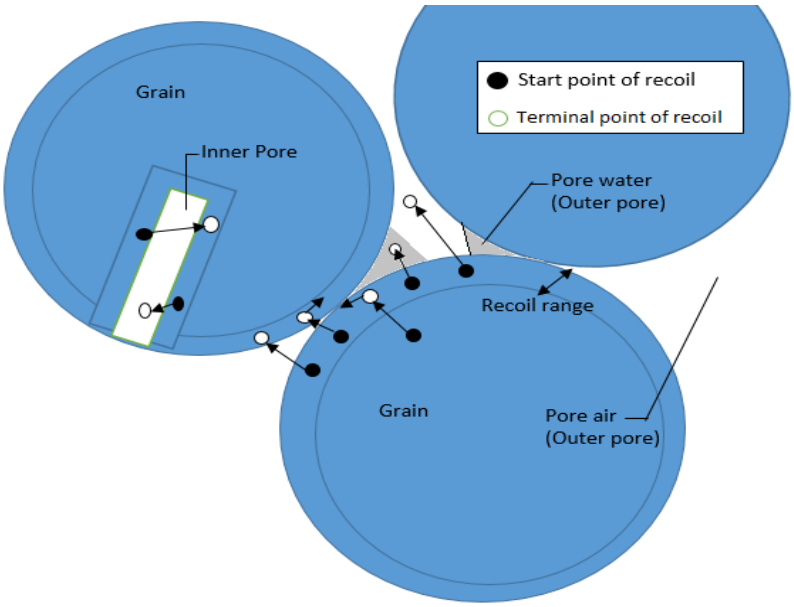


Figure 2.9: Schematic diagram of how radon emanates from soil grain [19].

Radon emanates more easily in a material that is more porous, therefore, its emanation would increase as a rock is crushed. That is because, a crushed rock offers an increased chance of radon emanation from individual mineral grains [20]. It is because of this logic that, rocks have lower radon emanation coefficients than soil. Even though radium distribution in a material is the key factor affecting the radon emanation coefficient , other factors such as soil porosity, moisture, grain size, temperature and atmospheric pressure can have an influence [20].

2.8.2 Radium distribution, soil moisture, porosity and grain size

Radium (^{226}Ra) is the direct source of radon and as such, its content in the soil is a key factor in determining the soil radon level and radon exhalation from the soil surface. This is because the radium content is directly proportional to the radon exhalation. Radium content is measured in Bq/kg that is, the activity concentration per unit mass [23].

Water is a more effective medium for stopping radon atoms within the pore space because recoil ranges in water are relatively less than in air, see Figure 2.9 and Table 2.2. It is important to note that the amount of moisture content that gives the maximum level of

emanation depends on the type of soil, porosity and its grain size [21].

Soil porosity is the ratio of the volume of air and water in soil pores to the total soil volume. Large pores reduce the the number of radon atoms entering nearby grains [23]. Small soil particles have a greater specific area which enhances emanation as the radium atoms will be much closer to the surface of the particle.

Table 2.2: Projected range of radon atoms in different mediums.

Medium	**Density (g/cm^3)**	**Projected range of ^{222}Rn atoms (nm)**
Air	1.58×10^{-3}	53×10^3
Water	1.00	77
Quartz (SiO_2)	2.65	34

2.9 Radon entry into a house

High levels of ^{222}Rn concentrations were discovered in Swedish houses in 1956 [24]. These concentrations were first thought to have been attributed to building materials because they were made of alum-shale concrete having elevated radium content. It was however, discovered in later studies that the high ^{222}Rn concentration came from the soil under the houses [25]. This has since led to more studies being carried out over the years to determine the factors which influence the indoor radon concentration.

Radon is drawn into buildings because the air pressure inside buildings is usually lower than the ground beneath. Drains and cracks in the foundation and slab, gaps around pipes and other openings provide points of entry of radon into a house, see Figure 2.10. The concentration of radon in indoor air is not constant but varies with time and the concentrations also vary between adjacent homes. Because of these fluctuations, it is therefore ideal to estimate the annual mean concentration of radon in indoor air by conducting measurements of at least three months to estimate the average values in a given area/house [18].

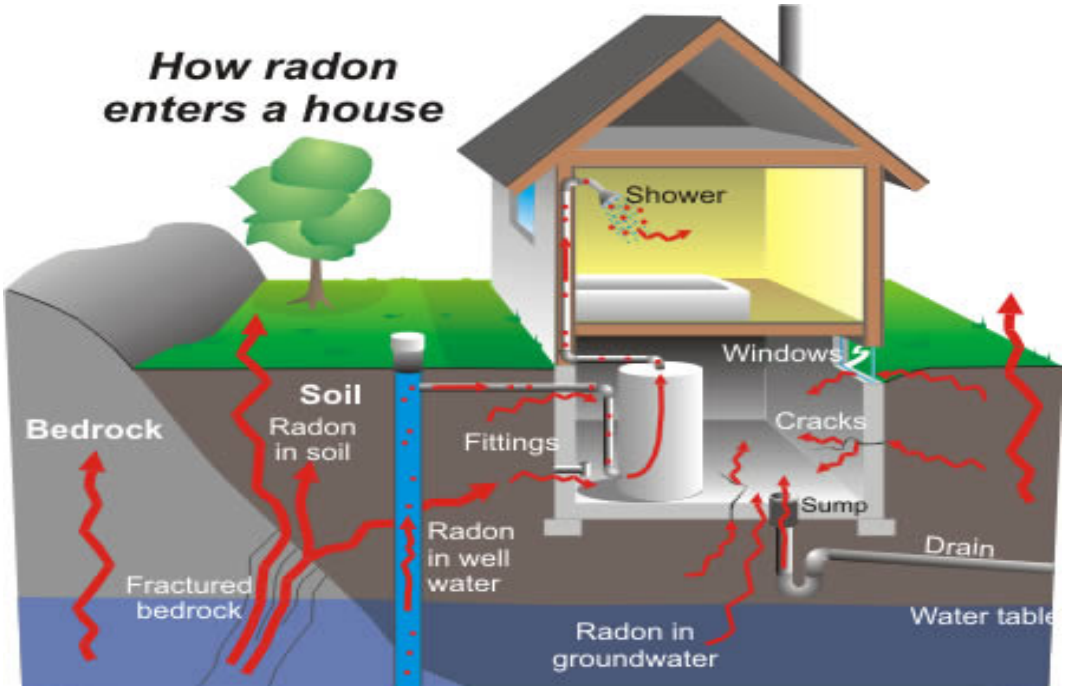


Figure 2.10: Radon pathways into a house [26].

2.9.1 Factors influencing radon concentration levels indoors

The concentration of radon in a home depends on a number of factors as follows [8]:

- The amount of uranium in the underlying rocks and soils.
- The rate of exchange between indoor and outdoor air.
- The routes available for the passage of radon from the soil into the home.
- The ventilation habits of the inhabitants and the air-tightness of the building.
- The building materials used in the construction of the house.

2.10 Risks of exposure to radon

Radon and its daughters pose a health risk if ingested or inhaled as it decays inside our bodies. The α-radiation emitted during radon decay is capable of splitting water

molecules thereby creating free radicals (e.g OH^-). These free radicals are very reactive ions which can damage the DNA of cells lining the walls of the lungs and thus cause lung cancer, as depicted by Figure 2.11 [23].

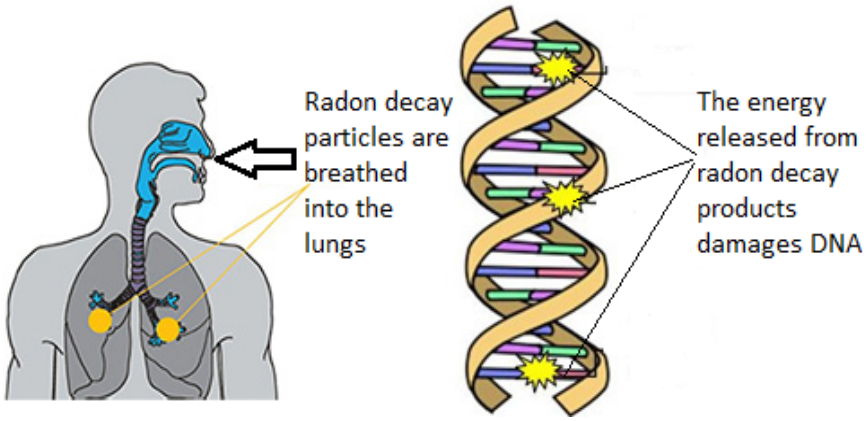


Figure 2.11: Health risk of exposure to radon gas.

Studies have been carried out in Ireland where it has been estimated that about 13 % of all annual lung cancer deaths in Ireland are caused by radon. The main conclusion reached was that active smokers' risk to lung cancer from radon was observed to be 25 times greater than the risk to non-smokers [27]. It is also important to note that radon can dissolve in water and be ingested, in this case other organs such as the kidney and bone marrow may receive low doses. And even low doses can be accumulative and result in cancer [28].

2.11 Dose quantities and Calculations

Definitions of some radiation quantities and units have changed over time but their purpose is to help quantify how much radiation one is exposed to and in setting limits for radiation protection. Absorbed dose is the amount of energy absorbed by any material per unit mass of material. It is measured in Gray (Gy), where 1 Gray is equivalent to 1 joule of energy deposited in one kilogram of a material (1Gy = 1J/kg) [29]. Mathematically, absorbed dose is given by equation 2.6.

$$D_T = \frac{\delta E}{\delta m}, \tag{2.6}$$

where D_T is the absorbed dose, δE is the energy absorbed in Joules (J) and δm is the mass of the material in kilograms (kg).

Equivalent dose (H_T) is the sum of absorbed doses in an organ or tissue from all contributing radiations of different types multiplied by their respective radiation weighting factors (W_R), see Table 2.3 showing the type of radiations and their weighting factors. The formula for calculating equivalent dose is given by equation 2.7.

Table 2.3: Type of radiations and their respective radiation weighting factors [29].

Type and energy range	**Radiation weighting factor (W_R)**
Photons, electrons and muons, all energies	1
Protons, other than recoil proton energy > 2 MeV	5
Alpha particles, fission fragments and heavy nuclei	20

Equivalent dose is measured in Sievert (Sv) and it relates the effective biological damage to the absorbed dose [30].

$$H_T = \sum W_R \times D_T, \tag{2.7}$$

where (H_T) is the equivalent dose in Sv, W_R is the radiation weighting factor and D_T is the absorbed dose.

Sensitivity of organs and tissues to radiation varies and as such a tissue weighting factor (W_T) has to be put in place. The tissue weighting factor refers to the fraction of the total stochastic risk due to the exposure of an organ. This stochastic risk, can be defined as the probability of radiation inducing some health effects [30]. Table 2.4 shows the different organs and their tissue weighting factors. This weighting factor is important in determining the effective dose received by an individual.

Table 2.4: Different organs and their tissue weighting factors [29].

Organ or Tissue (T)	Weight factor (W_T)
Oesophagus, Thyroid	0.04
Salivary glands, skin	0.01
Red bone marrow, stomach, lungs	0.12

The effective dose (E) is the sum of equivalent doses in all specified tissues and organs of the body and it is measured in Sievert (Sv). The general formula for calculating effective dose is given by equation 2.8:

$$E = \sum W_T \times H_T \tag{2.8}$$

The annual effective dose from inhalation of radon is determined by an expression derived from UNSCEAR [5] and it is given by:

$$H = C_{Rn} \times F \times T \times (DCF), \tag{2.9}$$

where

- H is the annual effective dose in (mSv)
- C_{Rn} is the average radon concentration in Bq/m^3
- F is the average equilibrium factor for radon and its progeny and has a value of 0.4
- T is the time in hours in a year (7000 hours) and
- DCF is the dose conversion factor which has a value of 9 nSv/Bqm^{-3}h.

The ICRP Publication 65 recommends that an action level of 200 - 600 Bq/m^3 be used for protection against radon in dwellings, this corresponds to an annual effective dose of 3 - 10 mSv, assuming 7000 hours per year spent at home [31].

2.12 Available literature

A number of studies have been conducted in various places around the world on indoor radon concentration levels. Surveys were carried out to find out, the distribution of residential radon concentration by most countries of the Organization for Economic Co-operation and Development (OECD) [28], see Table 2.5. Areas which have uranium-rich underlying rocks were found to have higher radon concentration levels, for example, from the table, Mexico has a higher radon concentration level because it is in a hilly region.

Table 2.5: Residential radon concentration levels in some countries in the OECD [28].

Indoor Radon Levels (Bq/m^3)		
Country	**Arithmetic mean**	**Geometric mean**
Australia	11	8
Canada	28	11
Denmark	59	39
Finland	120	84
Hungary	82	62
Japan	16	13
United Kingdom	20	14
USA	46	25
Sweden	108	56
Mexico	140	90

A study on airborne radon levels in Paarl houses (South Africa) was carried out using electret ion chambers and gamma-ray spectrometry [32]. Radon levels were measured in a hundred homes in a period of six months spanning through the spring and summer seasons in the Western Cape, South Africa. The radon concentration level found varied between 28 and 465 Bq/m^3, showing that houses having wooden floors had on average significantly higher radon levels than houses with cement floors. Higher radon levels were found in houses on or near the foothills of Paarl Mountain, which is made of granite outcrops containing above-average values of uranium. So from the findings, it was concluded that the geology of the area and the building materials used for the house construction affects the indoor radon concentration level.

Another study was conducted to assess the concentration of radon and its progeny in

air in the dwellings of Moradabad of Western Uttar Pradesh [8]. Passive monitoring devices called LR-115 plastic track detectors were used. Measurements were taken in 66 residential houses for a year by hanging twin cup radon dosimeters at a height of 1.5 cm - 2.0 m from ground level. The radon concentration levels obtained varied from 18.14 Bq/m^3 to 22.62 Bq/m^3. The highest radon concentration was recorded in winter and lowest in summer, this may have been due to ventilation condition in summer and winter being different. The obtained concentrations were well below the ICRP recommendations [8].

Radon prediction models are quite useful in understanding the factors influencing radon entry rates and determining the radon potential of new building sites. A linear regression model was developed in 2005 in Denmark to predict the annual average radon concentration in Danish houses [33]. The model used a number of variables such as house type, floor measurement, soil type and type of building materials used. Geology of the area and house construction being the main ones. The model also included seasonal variation corrections.

3

Experimental Methods and Data Analysis

3.1 Introduction

In this chapter, we look at the sampling strategy and the two main methods used in the current work to measure the indoor radon concentration levels. The chapter also gives a detailed background information on the equipment used, data analysis resulting from these equipment and an insightful description of the sampled houses. In addition, two other complimentary analysis techniques will be discussed in this chapter.

3.2 Description of the Study Area

Serule is a village in the central district of Botswana, around 350 km north of the capital Gaborone, with latitude 21°56'60 S and longitude 27°18'0 E. In 2007, Serule was proposed for the mining of uranium by A-Cap Resources Ltd Company, with a lease mining area of 70 km^2 after discovering some uranium deposits [10]. The licensed company estimated roughly about 158 million pounds of uranium to be found around the Serule area. See Figure 3.1 of the A-Cap Resources demarcations of the licensed areas.

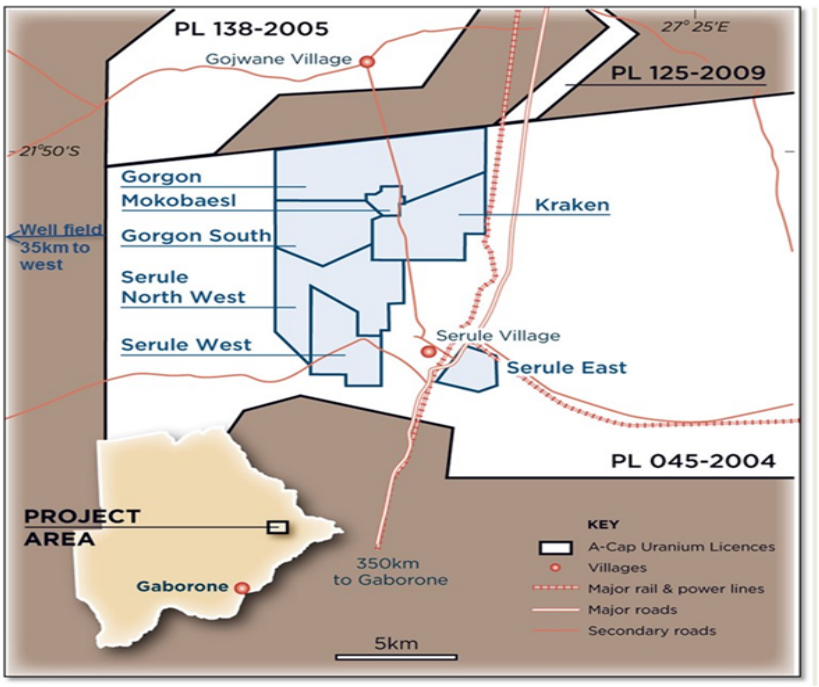


Figure 3.1: A-Cap Resources Uranium mining licensed area demarcations in Serule [34].

Serule is a rural community engaged in arable and livestock farming. It has a small population of about 3 756 according to the Central Statistics Office in 2011 [35]. The climate in Serule is semi-arid with rainfall in summer of about 440 mm/annum. The average temperature of Serule is about 20.4 °C, with the warmest month being January having an average temperature of 25.2 °C and July being the coldest month with an average temperature of 13.2 °C.

3.2.1 The Area of Interest

In this study, ten houses were randomly selected in Serule. Six houses within the A-Cap Resources mining area (that is, from SH1 to SH6) and four houses outside the licensed mining area (that is, from SH7 to SH10) see Figure 3.2. A Global Positioning System (GPS) was used to mark and identify the Serule Houses (SH) whose GPS points were needed for later referencing, see Figure 3.2 and Appendix A for more details. Two houses in Palapye, a town 80.1 km from the study area, were used as the control, that is PH1 and PH2.

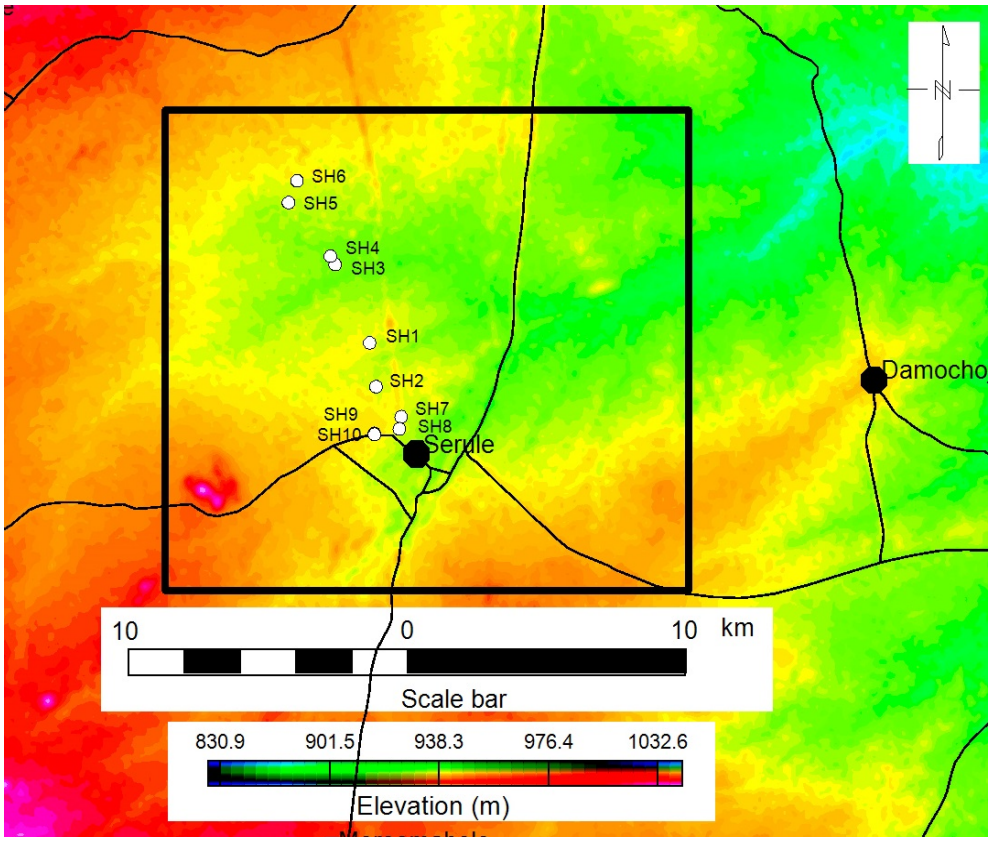


Figure 3.2: Sampling points (white circles) of the selected Serule homes used for the study as obtained from the GPS, SH9 and SH10 are in close proximity.

3.2.2 Materials used for the construction of the houses

The selected houses had varying construction materials, ranging from mud, brick, cement, planks to iron shed. Most of the houses being surveyed were made of cement with only two being of mud type. It is important to note that the mud used in the construction of the houses was mainly sourced locally in the area. Table 3.1 shows the building construction materials for each of the twelve houses used in the study. Figure 3.3 further shows actual photographs of some of the houses used in the current study.

Table 3.1: The building materials used in the construction of selected houses

Location	Within (W)/Outside (O) mining area	Floor type	Wall type
SH1	W	Cement	Plastered
SH2	W	Mud	Mud
SH3	W	Cement	Planked
SH4	W	Cement	Plastered
SH5	W	Cement	Plastered
SH6	W	Cement	Iron shed
SH7	O	Tiled	Plastered
SH8	O	Tiled	Plastered
SH9	O	Tiled	Plastered
SH10	O	Cement	Mud + Brick
PH1	O (Palapye)	Tiled	Plastered
PH2	O (Palapye)	Tiled	Plastered



(a) (b)

(c) (d)

Figure 3.3: Examples of some of the selected Serule houses, where radon measurements were conducted: (a) is made out of planks; (b) is a brick house with plastered walls; (c) is a plastered brick house; and, (d) is a red brick house with plastered walls.

3.3 Principles of Radon Detection Systems

The main measurement technique used in this work is an integrative passive method. Radon detection and measurement depends on counting alpha-particles of radon and its daughter products. Both active and passive radon monitors are available for this purpose.

Active radon monitors record the radon concentration in real-time. The measurement methods include using scintillation cells, in which the cells are covered in a scintillator, usually silver doped zinc sulphide (ZnS:Ag). The light pulses produced are recorded by a photomultiplier tube and associated electronics [17]. Another active measurement is by using ionization chambers, which allow filtered air to diffuse into the chamber and the current produced by ionization of the gas inside the chamber is detected. The measured ionization is caused by the decay of radon and its progeny. An advantage of this technique is that pulses caused by different decay products and radon can be distinguished. Electrostatic collection of decay products involves using a solid state detector to measure alpha particle energies. The detector is raised to a high voltage in order to collect the charged radon decay products as they are formed.

Active monitors like RAD7 and AlphaGuard are ideal for measuring indoor radon concentration since they are capable of simultaneously measuring temperature, air pressure and humidity along with the radon concentration [1]. An AlphaGuard also has high detection efficiency, a large measurement range, a high storage capacity and it is able to respond quickly to variations in radon concentration [36].

Passive measurement methods include using charcoal detectors. Activated charcoal adsorbs radon which then decays, the decay products formed will be retained allowing the adsorbed radon to be measured by gamma spectrometry of the emissions from ^{214}Pb and ^{214}Bi. Electret ion chambers (EIC) are passive radon detection monitors which were used in this work, this technique will be discussed in the next section. Etched track detectors are passive detectors which depend on the use of a plastic material to record the tracks of alpha particles from radon and its decay products. The damage/tracks created can be revealed later by etching the plastic material in a solution of hot sodium hydrox-

ide (NaOH). The number of tracks is counted by using a computerized program, which scans the microscopic picture of tracks. These detectors are generally used for long term measurement of radon concentration from a month to a year [17].

3.3.1 The E-PERM system

The E-PERM (Electret-Passive Environmental Radon Monitors) detectors are portable, passive and integrating ionization chambers that do not require an external source of power [37] or a battery for operation. E-PERMS were the main instrument employed in the present study. The E-PERM system is a combination of various components, see Figure 3.4, that is, the ion chamber which is made out of an electrically conductive plastic, the second component is an electrically charged Teflon disk called an electret that can be mounted on the chamber. The electret reader measures the surface voltage of the electret [37].



Figure 3.4: The Electret Passive Environmental Radon Monitor system.

The EIC can measure both short-term and long-term radon concentration in air, water and radon emanating from soil. Advantages of the system include the fact that it is minimally affected by changing temperature and relative humidity, as well as its ability to integrate measurements [37]. The E-PERM system was primarily developed for measurements of radon in houses.

3.3.2 Operation of the Electret

An electret is a dielectric material which has a surface charge that produces a strong electrostatic field capable of collecting ions of opposite signs. The electret is electrically charged with an initial electret voltage of about 750 Volts and it is then screwed into a semi-closed chamber volume so that the electret produces an electrostatic field [38]. The α-decay of radon and its daughter products produces α-particles with energies of about 5-7 MeV. This energy is lost when the positive α interacts with atomic electrons in the air. The electrons that result from ionisation are attracted to the positive electret thereby causing a reduction in the voltage [37].

The reduction in charge of the electret over a certain time is related to the integrated radon concentration. There are three types of electrets that are manufactured for different purposes. They are colour coded and have different thicknesses for their use in long-term (LT) or short-term (ST) measurements [37] . Electrets are very sensitive in such that they can be damaged if touched by hand, dust or fibers and rendered useless. It is therefore for this very reason that electrets are covered by a protective cap when they are not in use, see Figure 3.5 below of electrets. When electrets are exposed to ionizing radiation the surface charge also reduces.



Figure 3.5: Electrets manufactured by Rad Elec Inc.

3.3.3 The E-PERM Electret Ion Chamber

There are a number of electret ion chambers available commercially but the three most commonly used are the “S”, “L” and “H” chambers, see Figure 3.6. The S chamber is

used for short-term measurements of about 2-7 days and has a volume of 210 ml. The L chamber is used for long-term measurements and has a volume of 50 ml. The H chamber is the most sensitive to radon gas and has the largest chamber volume of 960 ml. The S chamber may be used with either the long-term (LT) or short-term (ST) electrets [38]. In this study, S chambers were used with LT electrets.



Figure 3.6: Chambers manufactured by Rad Elec Inc.

The E-PERM chambers are made of electrically conducting plastic that minimizes the response to the natural environmental γ-radiation. When the chambers are in storage or not in use, they are placed in the "off" position and when the E-PERMS are used, the chambers are turned to the "on" position by unscrewing the top screw cap, see Figure 3.7 below of the "on" and "off" position of the E-PERM chamber.

The S-chamber is designed in such a way that it has a filter inlet which allows radon into the chamber while it excludes or filters out radon progeny or environmental ions. The progeny filter is placed directly over six small holes that allow radon gas to freely diffuse in and out of the chamber, see Figure 3.8 [37].

When radon decays by α emission, the charged α-particles ionize the air within the chamber causing a production of ions. The electret at the bottom of the chamber collects only the ions produced inside the chamber and not the radon itself. The electrostatic field produced, causes a reduction of the charge on the electret [37]. Over some time, the depleted charge of the electrect becomes equal to the time integrated charge produced by

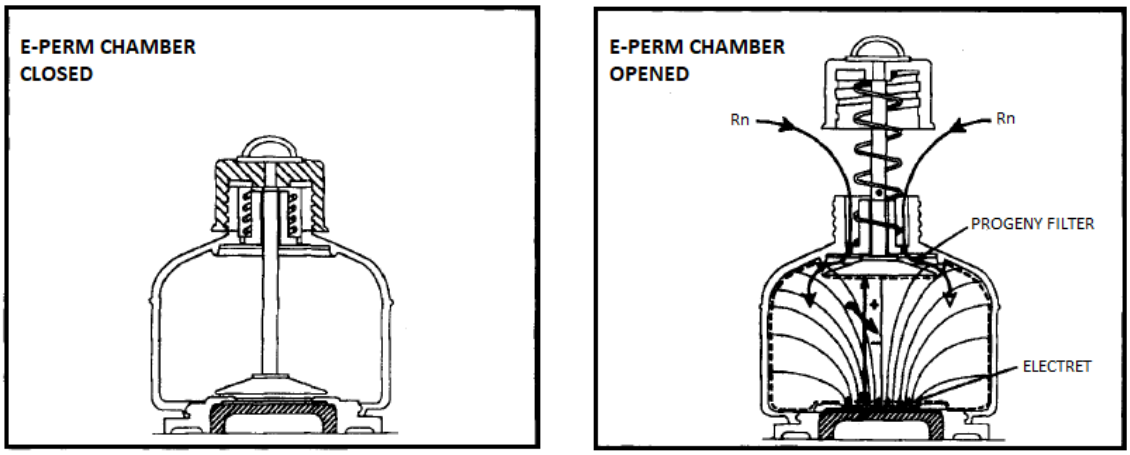


Figure 3.7: The E-PERM S-chamber in a closed position during storage or when not in use and during radon measurement when in an open position.

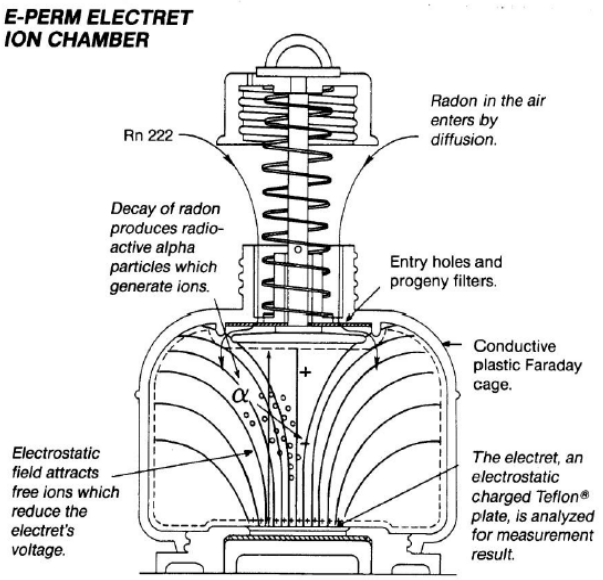


Figure 3.8: The mechanism of radon entry into the E-PERM S-chamber.

radon and its decay products. This in-turn is directly proportional to integrated radon concentration over that period, as already mentioned. The charge on the electret before and after the exposure is measured by a sensitive electret voltage reader.

3.3.4 Electret Voltage Readers

The electret voltage readers, also known as surface potential voltmeters are used for measuring the surface voltages of the electrets before and after exposure. The surface voltage change gives the radon concentration during the exposure period. There are two types of electret readers commercially available, the SPER-1 (Surface Potential Electret Voltage Reader) and SPER-2. The main difference between the two is that, the SPER-2 reader has an option to connect to a power supply and has a built-in microprocesssor for data storage [38]. In this study the SPER-1 electret reader was used. See Figure 3.9.

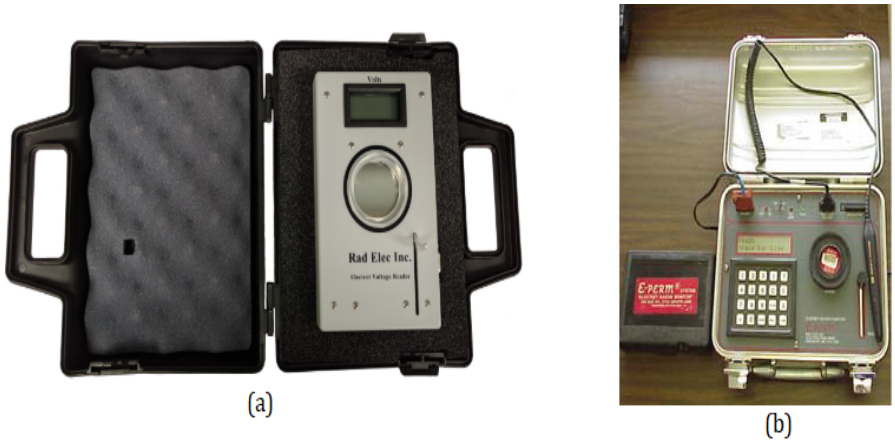


Figure 3.9: Figure (a) shows SPER-1 voltage reader and Figure (b) shows SPER-2 Voltage reader.

During measurement, the electret is placed face down into the circular receptacle on top of the SPER reader. The shutter window can be retracted and released allowing the reader to take measurements. Details on how radon concentration is calculated from the reduction in charge can be found in Appendix B.

3.4 Measurement of radon concentration levels using E-PERMS

The radon concentration levels were measured using the E-PERMS as discussed in the previous sections. Two E-PERM systems were deployed in each dwelling and placed at heights between 120 cm and 220 cm see Appendix A. A string was tied on the top cap of the E-PERM chamber and the chamber was hung at an ideal height ensuring that it did not disrupt the daily routines of the residents, see Figure 3.10 of how the E-PERMS were typically mounted in a house.



Figure 3.10: Typical example of how the E-PERM chambers were mounted in a house.

The radon concentration level measurements started in October 2018 and ended in July 2019, spanning through three seasons that is, summer, autumn and winter. However, data was only collected on six occasions over that time period, that is, in November 2018, January 2019, March 2019, April 2019, May 2019 and July 2019. The initial voltages on the electrets before deployment were read using the electret reader and recorded, see record sheet in Appendix B. It was also important to take note of the background radiation in the selected areas because a background correction has to be done when using E-PERMS. This is to correct for the contribution of environmental gamma rays to the reduction in the electret voltage.

A 6150AD automess dose rate meter was used to measure the background radiation. The automess is a hand-held monitor which has a built in Geiger-Muller tube for measuring photon radiation (gamma and X-radiation) [39]. It measures the dose rate in µSv/hr and hence a conversion factor had to be employed to change the units to µrad/hr and then finally to Bq/m^3. A background of 0.1 µGy/h (10 µrad/h) was measured to be equivalent to a concentration of 32 Bq/m^3 [37].

The following conversions were used [32, 37];

$$1\mu\text{Sv}/hr = 100\mu rad/hr \tag{3.1}$$

$$1\mu rad/hr = 3.2Bq/m^3 \tag{3.2}$$

The dose rate from the background gamma radiations from the twelve houses used in the study were recorded and expressed in units of Bq/m^3. The background values were subtracted from the other contributing parameters in order to find the radon concentration, see equation 3.3 , on calculating the radon concentration level [37].

$$C_{Rn} = \frac{\Delta V}{C_f \times t} - BG, \tag{3.3}$$

where,

- C$_{Rn}$ is the radon concentration in Bq/m^3
- ΔV is the change in voltage (Initial voltage - Final voltage) in V
- C$_f$ is the calibration factor in units V per Bqm^{-3} d. The calibration factor for long term (LT) E-PERMS is given by

$$C_f(LT) = 0.0000168 \times \frac{V_i + V_f}{2} + 0.00481 \tag{3.4}$$

- t is the time in days and

- BG is the environmental background radiation

The average indoor radon concentration levels for each of the twelve houses was also calculated using equation 3.3. In this case, the initial electret voltages from the very first day of deployement and the very final electret voltages were considered. The overall measurement period was also taken into account, that is, from the first day of deployment of the E-PERMS until when they were retrieved from the sampled houses. The values of the calibration factors used to calculate the radon concentration can be seen in more detail in Appendix B.

3.5 Soil sample collection and preparation

There are many factors that contribute to the amount of radon concentration in a house, as already established in section 2.9.1 of Chapter 2. One key factor is the amount of uranium in the underlying rocks or the radium content in the soil. It is therefore important to analyse the soil samples around the vicinity of the houses in order to determine the radiation concentration or radium content in the area.

Twelve soil samples, each a representative of the areas of interest were collected from the vicinity of the houses used in the current study. The samples were collected at a depth of 15 cm using an auger and placed in zip-locker polyethene bags as depicted in Figure 3.12. The auger was dusted off after every sample collection to minimize cross-contamination of the samples. The GPS coordinates of the soil samples were also recorded as in Table 3.2, with the sample location code. The Garmin GPS device, depicted in Fig. 3.11 was used in the current study.



Figure 3.11: The Garmin GPS device used in the current study.



(a) (b)

Figure 3.12: Soil sample collection using an auger

Table 3.2: Soil sample codes and their respective GPS coordinates.

Soil sample code	GPS coordinates
SSH1	S 21.88877° E 27.28854°
SSH2	S 21.90280° E 27.29088°
SSH3	S 21.86379° E 27.27662°
SSH4	S 21.86119° E 27.27495°
SSH5	S 21.84416° E 27.26041°
SSH6	S 21.83723° E 27.26334°
SSH7	S 21.91245° E 27.29969°
SSH8	S 21.91633° E 27.29902°
SSH9	S 21.91771° E 27.29019°
SSH10	S 21.91813° E 27.29036°
SSH11	S 22.51603° E 27.10512°
SSH12	S 22.56308° E 27.10729°

The samples were taken to the radiation storage room in BIUST where soil preparation began. Fig. 3.13 depicts the procedures followed in preparing the soil samples for measurement. A mortar and pestle were used to grind the soil samples, followed by sieving using a 2 mm standard sieve to a more homogeneous particle size. The samples were packaged and transported to iThemba Laboratory for Accelerator Based Sciences at the Environmental Radioactivity Laboratory (ERL) in Cape Town, South Africa. Before transferring the soil samples into sample holders, they were oven dried at 105 °C to get rid of moisture, see Fig. 3.13(b).

After drying, the samples were weighed and sealed in 50 ml pill bottles, see Fig. 3.13(c) and Fig. 3.13(d) and then they were stored in the laboratory while waiting for them to be

counted using the High Purity Germanium (HPGe) detector. The soil samples had a mass range of about 58 - 76 grams, as shown in Table 3.3. Some soil samples were originally finer than others even before sieving, causing the samples to have a mass difference as all the samples were filled to the brim of the pill containers. Finer soil samples had more mass than medium-sized ones.



(a) (b)

(c) (d)

Figure 3.13: Steps of soil preparation: (a) grinding of soil samples using mortar and pestle; (b) drying of soil samples in an oven; (c) weighing of soil samples after drying; and, (d) sealed soil samples awaiting counting.

Table 3.3: Soil sample codes and their respective mass in kilograms.

Soil sample code	Sample mass (kg)
SSH1	0.07554
SSH2	0.07133
SSH3	0.06150
SSH4	0.06360
SSH5	0.06925
SSH6	0.05814
SSH7	0.05885
SSH8	0.06650
SSH9	0.07396
SSH10	0.06868
SSH11	0.07454
SSH12	0.07151

3.6 Analytical techniques used on the soil samples

The two main techniques employed in this study for analysing soil samples are the radiometric analysis using the HPGe detector and the chemical analysis using the Inductively Coupled Plasma-Mass Spectrometry (ICP-MS). This was done to estimate the activity concentrations and radium content in the soil samples, and also determine the elemental composition of some selected samples.

3.6.1 The High Purity Germanium (HPGe) detector

The HPGe system in iThemba LABS used in the current work, is a GC4520 p-type Canberra system detector which is sensitive to gamma energy above 100 keV. It has a relative efficiency of 45 % , a 2.2 keV full width half maximum (FWHM) and an energy resolution at 1332 keV from ^{60}Co decay. The detector has a crystal height of a diameter of 62.5 mm and length of 59.9 mm. The system's detector crystal is housed within a 10 cm thick lead (Pb) castle to shield and reduce the contribution of background radiation.

The lead castle is lined with a thin layer of copper inside to attenuate the low energy X-rays brought about by the gamma rays in lead.

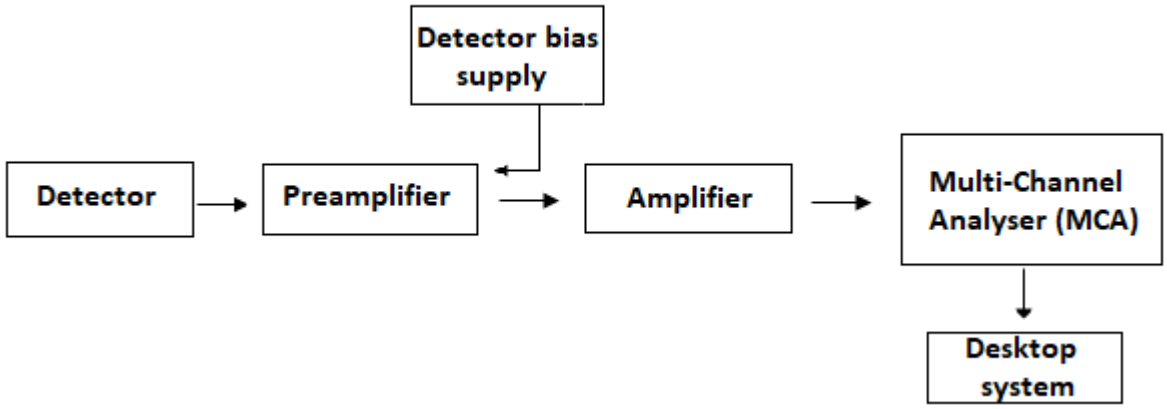


Figure 3.14: Schematic diagram of the HPGe system at iThemba LABS.

The schematic diagram in Figure 3.14 depicts how the HPGe system at iThemba LABS is assembled. The high voltage power supply facilitates the necessary voltage to the detector and the components of the system. The germanium crystal within the detector converts the gamma ray energy into an electric signal with a very small/minute voltage pulse, and because of this, the pulse is then passed through the pre-amplifier to magnify it. The pre-amplifier firstly has to separate the voltage pulse from the bias voltage through a mechanism called the Field Effect Transistor (FET) [40]. This mechanism works best at very low temperatures since reduced temperatures decrease thermal noise and also improve the resolution. Liquid nitrogen is therefore used to cool down the system's electronics to prevent the pre-amplifier from warming up and short circuiting because of the high bias voltage that passes through it.

The pre-amplifier gives an analog output signal with discrete pulses and the pulses strength corresponds to the energy of the individual gamma rays. The Multi Channel Analyser (MCA) is used to process these pulses from the amplifier. The signal is firstly converted from analog form to digital by an Analog-to-Digital (ADC) Converter and the ADC output signal is stored in the MCA memory. The digitized pulses are counted in specific channels of the MCA depending on the amplitude of the pulse which reaches the

ADC [40].

The Palmtop MCA software was used in the current work for the data acquisition and analysis of generated spectra. It consists of 8191 channels which store digital values and each channel records the number of pulses/counts of a given pulse energy. Pulses which closely follow one another are rejected once the ADC starts analysing a pulse, and this period of time when the ADC is not registering incoming pulses is called the dead time. The Palmtop MCA software provides the live time of the detector and the real time is corrected for by the dead time which the software provides (and it was around 0.01 - 1% in this study). A standard source (e.g ^{60}Co, ^{152}Eu, ^{232}Th and/or ^{238}U) is used for energy calibration and detector efficiency and thereafter measurement of background and samples can be carried out.

3.6.1.1 Energy calibration for Gamma Spectrometry

Energy calibration is deriving a relation between peak pulse height (MCA channel number) and gamma-ray energy in physical units. To carry out the energy calibration of the HPGe system, a standard source is used in which the gamma ray lines/photo-peaks are known [41]. For the current work, a ^{232}Th standard source was used for energy calibration, see Table 3.4 for the gamma-ray lines from^{232}Th.

Table 3.4: Gamma-ray lines from ^{232}Th used for energy calibration [42].

Nuclide	Gamma-ray energy (keV)	Branching ratio
^{228}Ac	129.065	0.0242
^{228}Ac	209.253	0.0389
^{228}Ac	338.322	0.1127
^{208}Tl	583.191	0.3036
^{228}Ac	911.205	0.2584
^{208}Tl	2614.533	0.1399

3.6.1.2 Energy calibration curve

The regions of interest (ROIs) were selected, that is, the gamma-ray photo-peaks for ^{232}Th and the channel numbers were converted to energy, see Table 3.5. The relationship between channel number and energy gives a linear relation as depicted by Figure 3.15.

Table 3.5: MCA channel numbers and their corresponding gamma-ray peaks from ^{232}Th.

Channel number	Gamma-ray energy (keV)
247	129.065
400	209.253
646	338.322
1114	583.191
1740	911.205
4994	2614.533

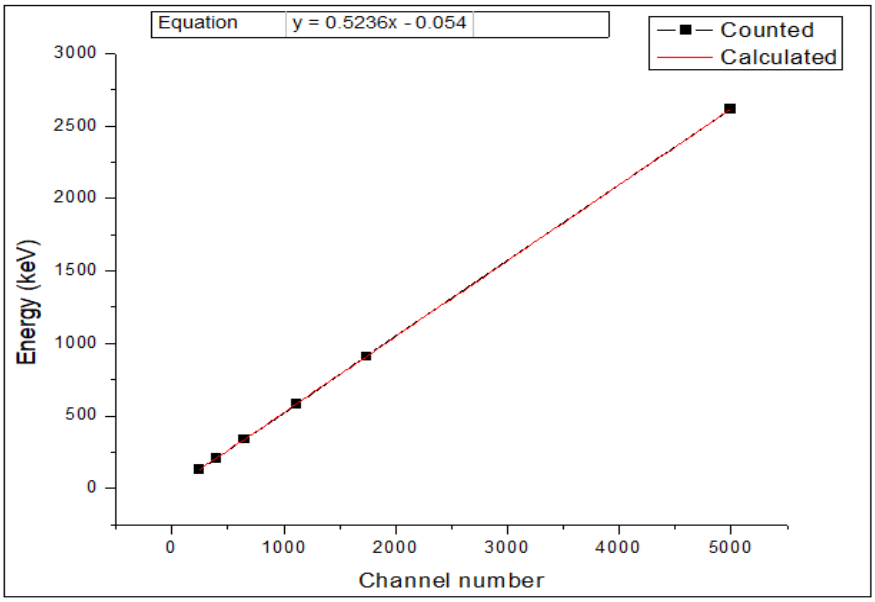


Figure 3.15: Energy calibration curve showing the relation of channels and energy.

3.6.1.3 Full energy peak efficiency calibration

Detection efficiency is a ratio of the number of photons observed by the detector with respect to the number of photons emitted by the source. The number of photons emitted by a radioactive source is normally larger than the number of photons detected by the

detector. In this study, a full energy peak efficiency that relates the peak area at a particular energy to the number of gamma-rays emitted by the radioactive source was used. It is dependent amongst others on the geometrical configuration of source and detector. Two standard sources, ^{238}U ($\sim$ 4940 Bq/kg: IAEA/RGU-1) and ^{40}K ($\sim$ 16252 Bq/kg: KCl) were prepared and used.

These standard sources of uranium ore and KCl (Potassium Chloride) were prepared in 50 ml pill bottle sample holders. The sources were prepared in order to mimic the conditions of the soil samples to be measured, that is, the sample geometry and densities should not vary much as compared to the sources [41]. The standard sources were each counted for an hour (3600 s) using the ERL HPGe gamma-ray detector system. In Tables 3.6 and 3.7 , the gamma-ray lines used for calibration are shown for the ^{238}U and ^{40}K, respectively. Figure 3.16 represents the efficiency curve data as function of energy and the results of the power fit to the data. The data presented in Figure 3.16 were calculated for each energy using equation 3.5 discussed in more details in the follow-up subsection 3.6.2.

Table 3.6: Gamma-ray lines from ^{238}U used for efficiency calibration [42].

Nuclide	Gamma-ray energy (keV)	Branching ratio
^{226}Ra	186.10	0.0617
^{214}Pb	241.98	0.0750
	295.21	0.1850
	351.92	0.3580
^{214}Bi	609.31	0.4479
	768.36	0.0480
	938.06	0.0303
	1120.29	0.1480
	1238.11	0.0586
	1377.66	0.0392
	1729.60	0.0288
	1764.49	0.1536
	2204.21	0.0486
^{234m}Pa	1001.03	0.0084

Table 3.7: Gamma-ray line from ^{40}K used for efficiency calibration [42].

Nuclide	Gamma-ray energy (keV)	Branching ratio
^{40}K	1460.83	0.1067

The efficiency (ε_f) at a given energy E (keV), can be computed by:

$$\varepsilon_f = a \times (\frac{E}{E_o})^b \tag{3.5}$$

Where E (keV) is the energy of the gamma-ray, E_o = 1 keV, a and b are fit parameters, see also Figure 3.16.

The fit parameters determined as shown in Figure 3.16, were used to analyse the twelve samples which were counted for 10 hours each.

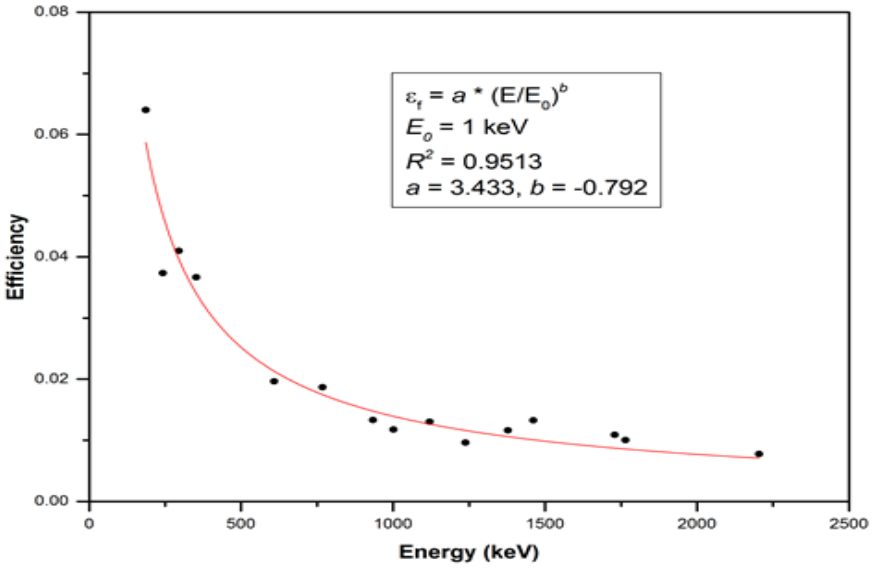


Figure 3.16: The efficiency curve of the ERL HPGe detector as a function of energy, showing the fit parameters from the ^{238}U and ^{40}K data points.

3.6.2 Calculation of activity concentrations

The main aim of using gamma spectrometry on soil samples is to identify the amount of radiation/activity per one kilogram of a given sample. The activity concentration, A

(Bq/kg) for ^{238}U, ^{232}Th and ^{40}K was calculated using equation 3.6 [43]

$$A = \frac{N}{\varepsilon_f \times I \times m \times t_s} \tag{3.6}$$

Where;

- N - (True counts) the corrected net peak area of a full-energy peak (that is, the net peak area in the sample spectrum minus the corresponding net peak area in the background spectrum.)
- ε_f - the efficiency at photo-peak energy
- I_γ - the branching ratio of the photo-peak energy.
- m - the mass (in kg) of the measured sample
- t_s - the live time of the sample spectrum collection in seconds

The activity concentration of each radionuclide contained in a given sample is obtained through gamma spectrometry. Figure 3.17 gives the observed radionuclides and their energies from one of the samples used in the current study.

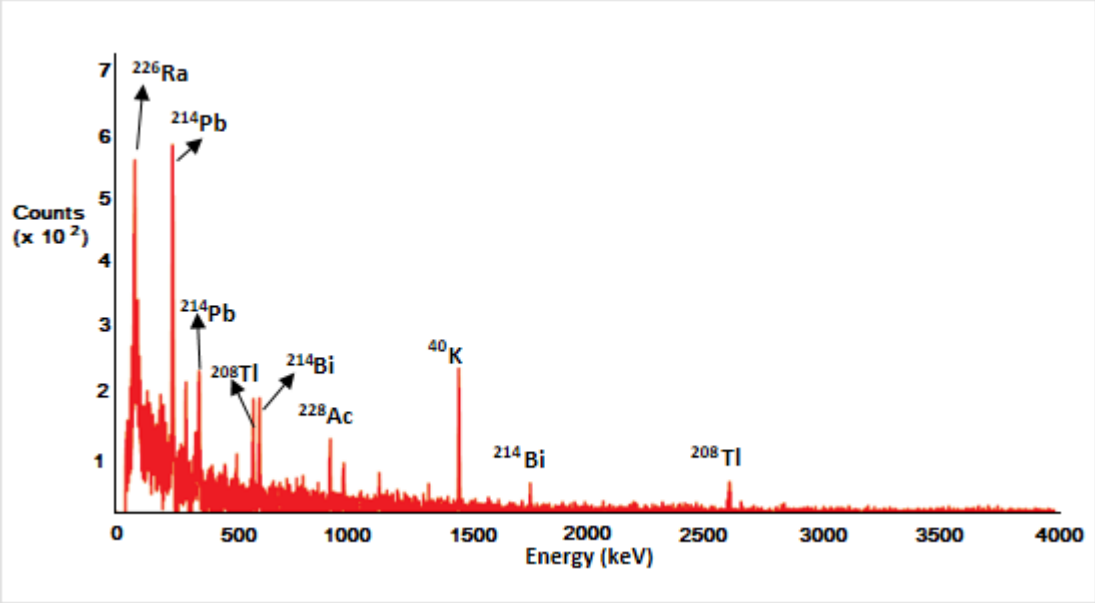


Figure 3.17: A spectrum of observed radionuclides from one of the soil samples used in the current study.

3.6.3 Radiological hazard effects

3.6.3.1 Radium Equivalent Activity

The radionuclides of ^{226}Ra, ^{232}Th and ^{40}K are not uniformly distributed in the soil, therefore the radium equivalent activity Ra_{eq} is introduced to identify uniformity [5]. The obtained values of Ra_{eq} are used in assessing the health hazards effects as a result of the activity concentration of ^{238}U, ^{232}Th and ^{40}K in the soil. Equation 3.7 was used to determine the value of Ra_{eq}.

$$Ra_{eq} = C_{Ra} + 1.43C_{Th} + 0.077C_K \tag{3.7}$$

Where C_{Ra}, C_K and C_{Th} are the activity concentrations of ^{226}Ra, ^{40}K and ^{232}Th in Bq/kg respectively. From equation 3.7, it is assumed that 4810 Bq/kg of ^{40}K, 259 Bq/kg of ^{232}Th and 370 Bq/kg of ^{226}Ra (^{238}U) produce the same gamma dose [5].

3.6.3.2 Absorbed dose rate

The health risk is evaluated by calculating the absorbed dose rate which human beings are exposed to. Dose conversion factors are applied to the measured activity concentration of ^{226}Ra, ^{232}Th and ^{40}K to change the concentration to doses. The conversion factors, 0.462, 0.0417 and 0.604 for uranium, potassium and thorium respectively are used [5]. The total dose rate (D) is calculated using equation 3.8.

$$D = 0.462C_{Ra} + 0.604C_{Th} + 0.0417C_K(nGyh^{-1}) \tag{3.8}$$

Where C_{Ra}, C_{Th} and C_K are the activity concentrations of ^{226}Ra, ^{232}Th and ^{40}K in Bq/kg respectively. The world average absorbed dose rate is given as 57 nGyh^{-1} [5].

3.6.3.3 Hazard indices

The hazard indices indicate external and internal radiation hazards. The set radiation dose limit is given as 1 mSv/yr. The external hazard index (H_{ex}) is given by equation 3.9 and should be less than or equal to 1 [44]. If it exceeds 1, it is a cause for concern.

$$H_{ex} = \frac{C_{Ra}}{370} + \frac{C_{Th}}{259} + \frac{C_K}{4810} \tag{3.9}$$

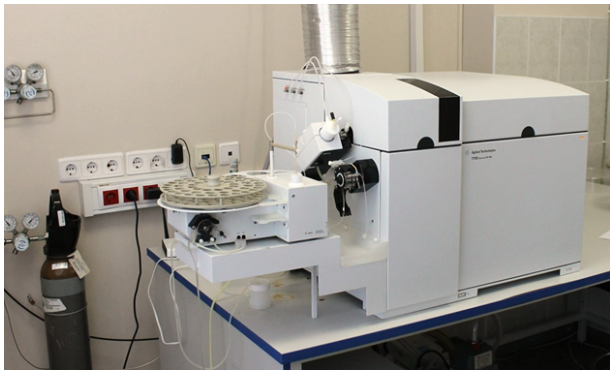
C_{Ra}, C_{Th} and C_K have their usual meanings. The internal hazard index (H_{in}) present the internal exposure to radon and its progeny/ daughter nuclides. The equation for H_{in} is given by equation 3.10 and it is also has to be less than or equal to 1 [44].

$$H_{in} = \frac{C_{Ra}}{185} + \frac{C_{Th}}{259} + \frac{C_K}{4810} \tag{3.10}$$

3.6.4 The Inductively Coupled Plasma Mass Spectrometry (ICP-MS)

The ICP-MS system is an instrument capable of analysing heavy metals in environmental samples. One of the advantages of this system is that it is capable of doing rapid multi-elemental analysis of soil, water, plant and even food samples. In the current work, ICP-MS was used to determine the elemental composition of some heavy elements in the soil samples collected. Only five soil samples were measured using this system, that is, SSH4, SSH6, SSH7, SSH9 and SSH12. This was done systematically because SSH4 and SSH6 are from within the mining area in Serule, SSH7 and SSH9 are in Serule but outside the mining area and SSH12 is a control in Palapye. These measurements were done in order to do a comparison with the results obtained from the HPGe. The ICP-MS measurements for this study, were carried out at the Central Analytical Facilities (CAF) at Stellenbosch University, South Africa, using an Agilent 7700x ICP-MS system, see Fig 3.18(a).

To carry out ICP-MS for the total elemental analysis of soil samples, suitable techniques of dissolution of the elements in the sample were developed. The samples were acid digested using a strong acid such as nitric acid (HNO_3). Samples were then microwave digested to extract the heavy metals from the soil, see Fig 3.18(b).



(a)



(b)

Figure 3.18: The ICP-MS system used in analysing the soil samples: (a) The Agilent 7700x ICP-MS with Octupole Reaction system; and, (b) The microwave digester used in sample preparation.

The digested soil samples were placed in ICP-MS system where they were disintegrated into atomic constituents followed by ionization in an argon plasma [43]. The mass filters in the mass spectrometer were used to separate the positively charged ions before they were measured using an ion detector.

The heavy metals of interest were lead (Pb), arsenic (As), mercury (Hg), zinc (Zn), cadmium (Cd), cobalt (Co), chromium (Cr), nickel (Ni) and copper (Cu). The chosen heavy metals have carcinogenic effects and hence the need to focus on them. The concentrations were given in µg/kg but were then converted to mg/kg see Appendix D for more details. It is important to note that 1 mg/kg = 1 ppm (parts per million). The ICP-MS results were also compared relative to the guidelines provided by WHO/FAO on the maximum allowable limit of heavy metal concentration in soil [45].

4

Results and Interpretation

4.1 Introduction

This chapter presents the results obtained in the present study. This will include, the levels of radon concentrations measured in each dwelling using the E-PERMS, the activity concentrations of identified radionuclides in collected soil samples using the HPGe gamma ray detector and the chemical analysis using the ICP-MS to determine the elemental composition of the selected soil samples.

4.2 Average Indoor Radon Concentration

The results presented on Table 4.1 and Figure 4.1 show the average indoor radon concentration. The highest average indoor radon concentration was recorded for both the SH4 and SH6 houses, with the average values of 40.0 ± 7.2 and 44.8 ± 4.6 Bq/m^3, respectively. Comparing houses within the mining area (SH1 - SH6) and those outside (PH1 - PH2), it can be observed as expected that, those within the mining area recorded relatively higher radon concentrations than those outside. PH1 and PH2 being the control, show quite low radon concentration in comparison to all the houses in Serule as depicted in Fig. 4.1.

Table 4.1: The average indoor radon concentration levels in the twelve selected houses.

Sample location	Average indoor radon concentration level (Bq/m^3)
SH1	22.1 ± 1.9
SH2	20.9 ± 2.8
SH3	26.2 ± 3.9
SH4	44.8 ± 4.6
SH5	30.0 ± 4.0
SH6	40.0 ± 7.2
SH7	20.2 ± 3.2
SH8	24.4 ± 3.5
SH9	15.7 ± 2.9
SH10	21.9 ± 3.2
PH1	6.8 ± 2.9
PH2	7.2 ± 4.1

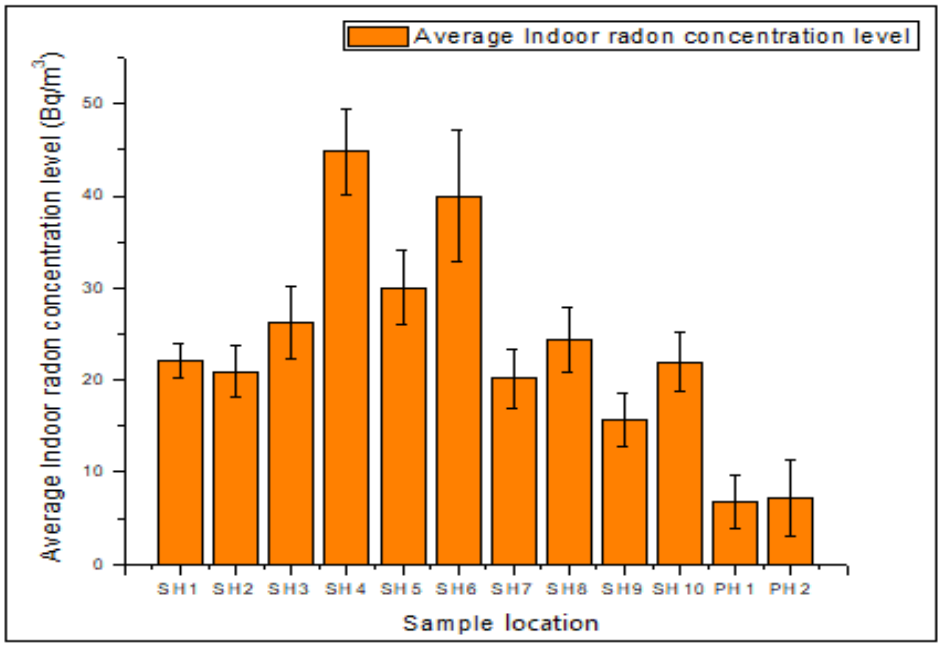


Figure 4.1: Average indoor radon concentration in the selected dwellings.

It can be observed that the distribution of radon concentration levels in Serule houses is

well below the IAEA set limit of 300 Bq/m^3 [4]. The weighted average radon concentration from all the ten sampled houses in Serule area was 23.4 ± 2.1 Bq/m^3 and from the control houses in Palapye, the average was recorded to be 7.0 ± 0.3 Bq/m^3. The results obtained agree with the available literature that, indeed the underlying rocks which are rich in uranium influence the radon concentration levels [28], as elevated concentrations are recorded in Serule area, a proposed mining area.

4.2.1 Monthly variations of radon concentration levels

The monthly indoor radon concentration levels were compared relative to the average radon concentration for each of the twelve houses. This was done to monitor the monthly variation relative to the calculated average value determined for each house.

Serule House 1 (SH1), recorded some fluctuations in the radon concentrations, with January having a slightly higher concentration than July, see Figure 4.2. However, it is safe to assume that SH1 experienced relatively consistent radon concentration levels since there is an overlap between the value of the average radon concentration and the monthly concentrations. Thus, the radon concentration levels can be assumed to have been constant (within uncertainties) during the monitoring period.

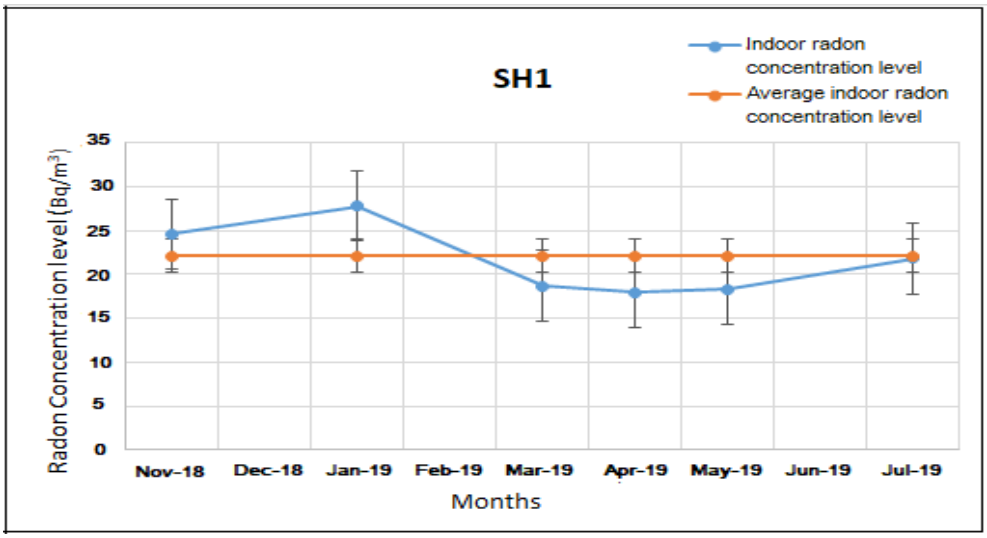


Figure 4.2: Distribution of indoor radon concentration levels in SH1 across the months relative to the average indoor radon concentration level.

There were distinct differences in the radon concentrations in SH2 over the months, see Figure 4.3, with July having a relatively high concentration compared to the average value.

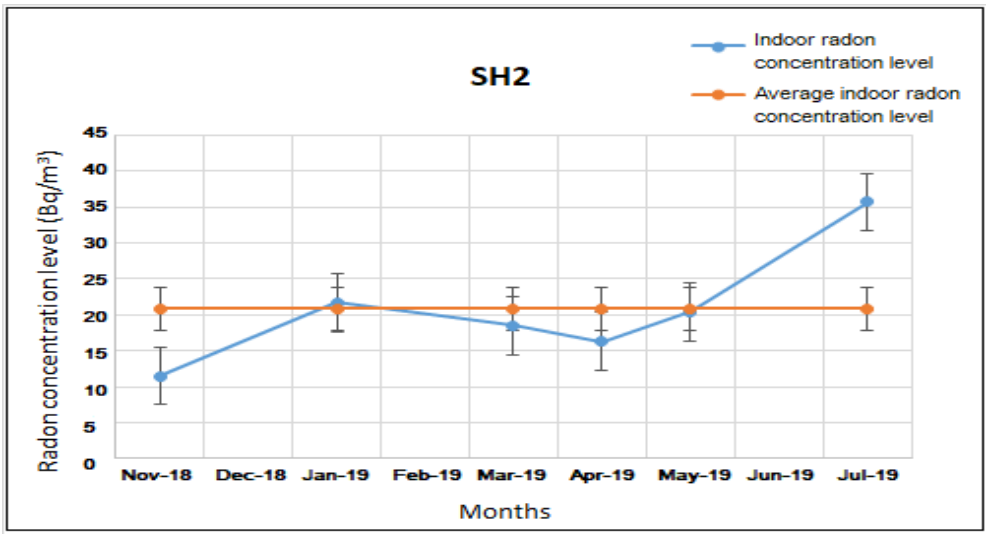


Figure 4.3: Distribution of indoor radon concentration levels in SH2 across the months relative to the average indoor radon concentration level.

SH3 recorded lower radon concentration levels from November to March monitoring period, and an increase from May to July, refer to Figure 4.4. SH4, SH5 and SH7 also follow a similar pattern as SH3, see Figures 4.5, 4.6 and 4.8 respectively.

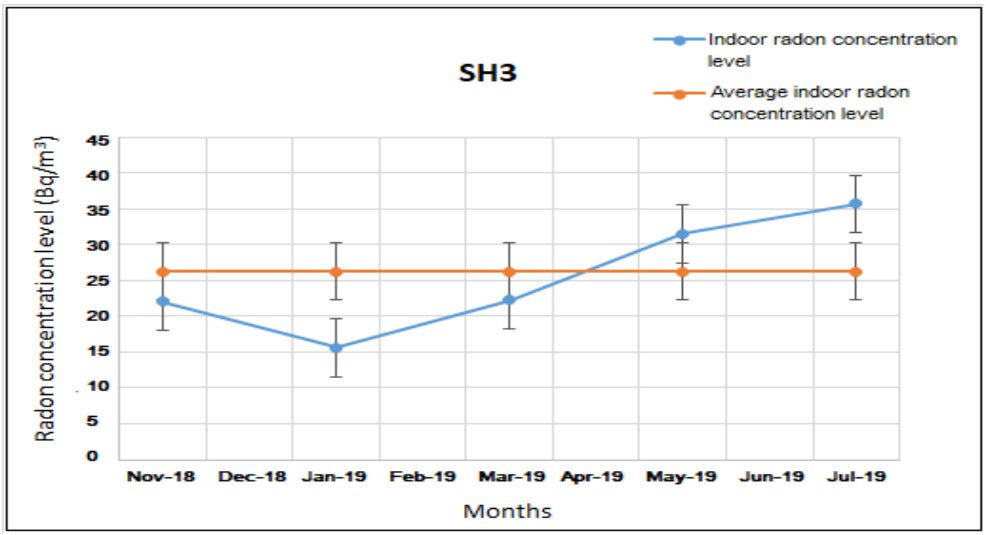


Figure 4.4: Distribution of indoor radon concentration levels in SH3 across the months relative to the average indoor radon concentration level.

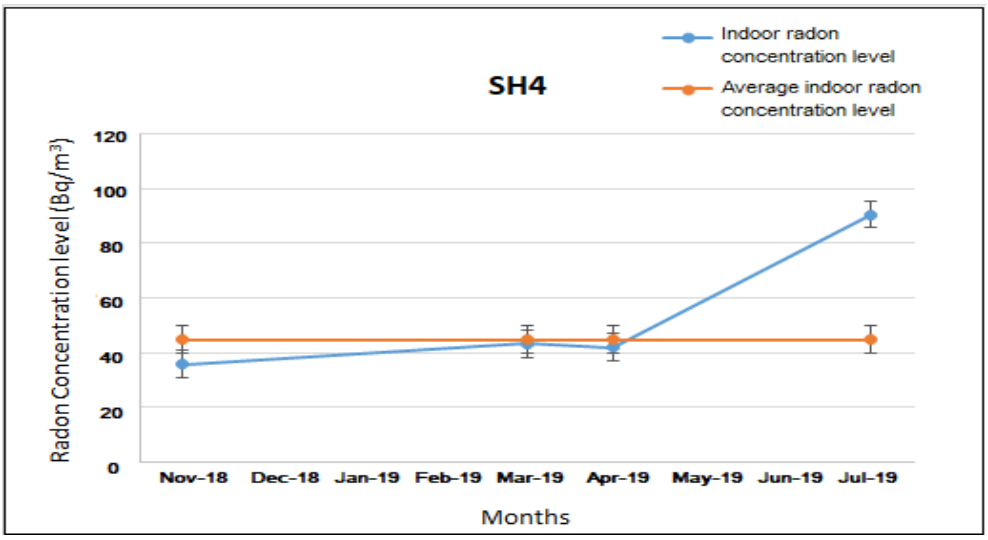


Figure 4.5: Distribution of indoor radon concentration levels in SH4 across the months relative to the average indoor radon concentration level.

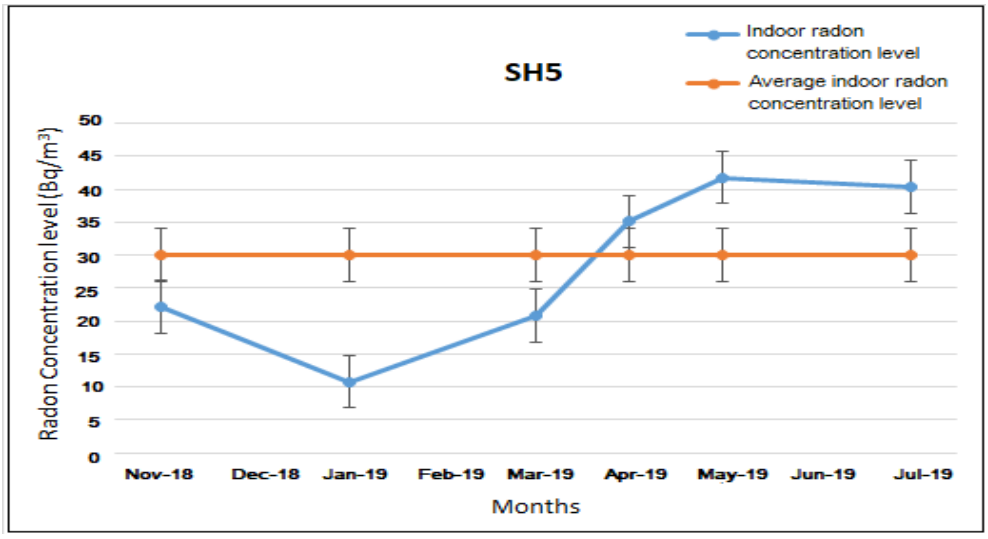


Figure 4.6: Distribution of indoor radon concentration levels in SH5 across the months relative to the average indoor radon concentration level.

SH6 (in Figure 4.7) show some fluctuations in the radon concentration but the overlaps between the average and the monthly values show that it generally experienced a concentration of about 40.0 Bq/m^3.

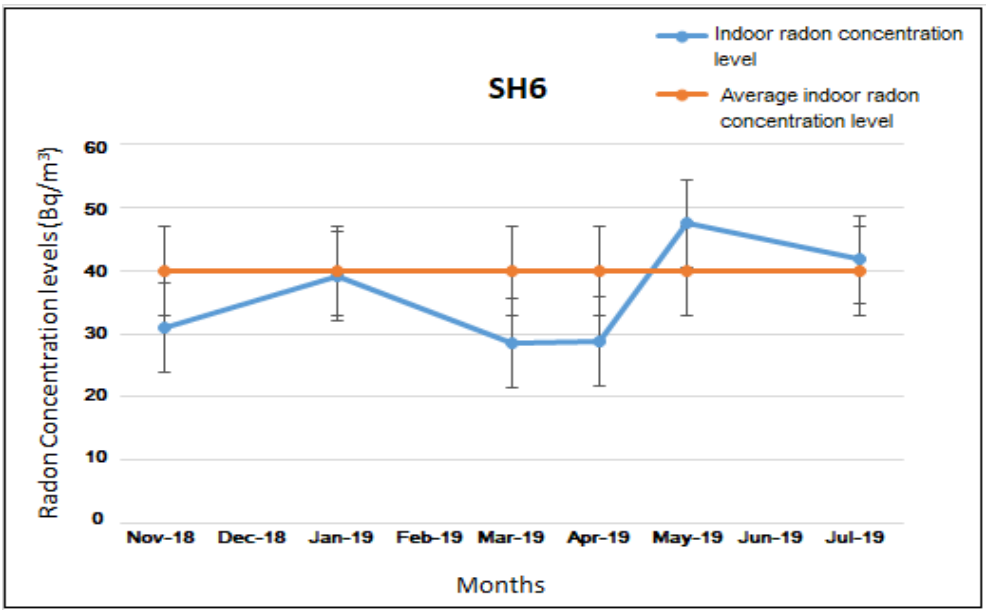


Figure 4.7: Distribution of indoor radon concentration levels in SH6 across the months relative to the average indoor radon concentration level.

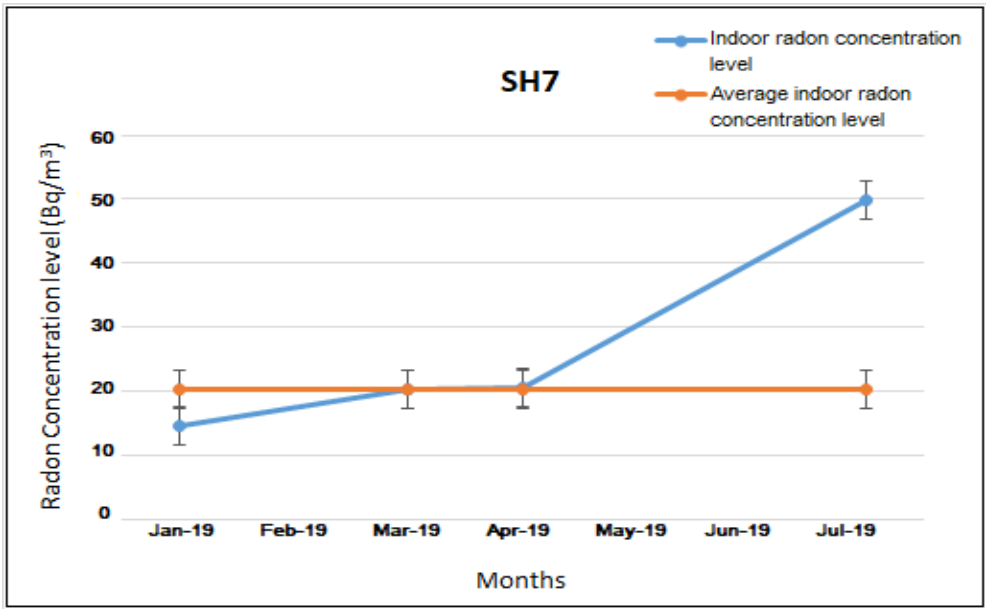


Figure 4.8: Distribution of indoor radon concentration levels in SH7 across the months relative to the average indoor radon concentration level.

SH8 recorded a relatively consistent radon concentration of about 24.4 Bq/m^3 from Nov-2018 to May-2019 because of the overlap in the average value and the monthly values, see Figure 4.9.

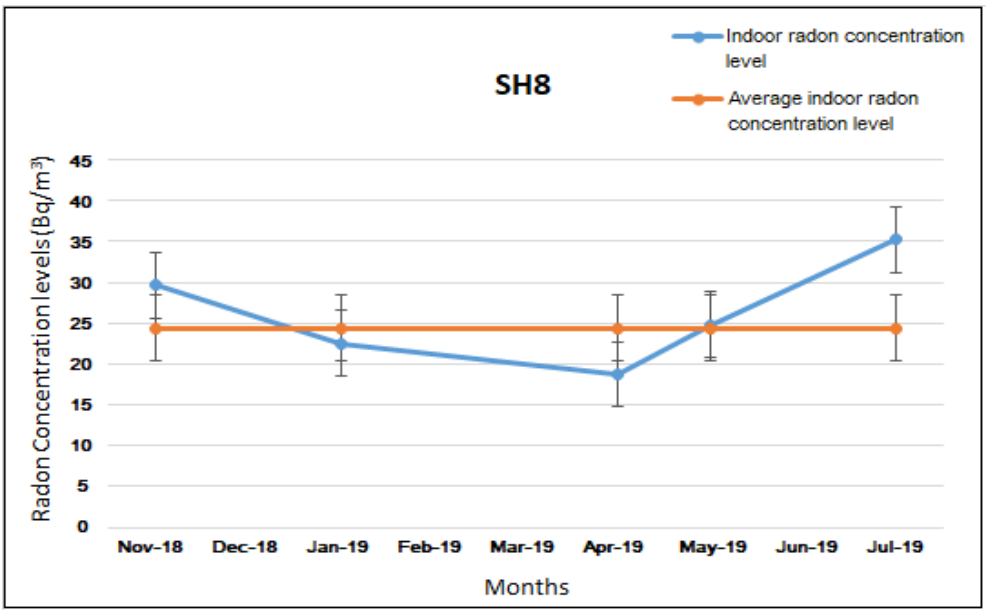


Figure 4.9: The distribution of indoor radon concentration levels in SH8 across the months relative to the average indoor radon concentration level.

SH9 (Figure 4.10) recorded a big reduction in the radon concentration in March than any other month but generally had concentrations that did not deviate much from the average which was about 15.7 Bq/m^3.

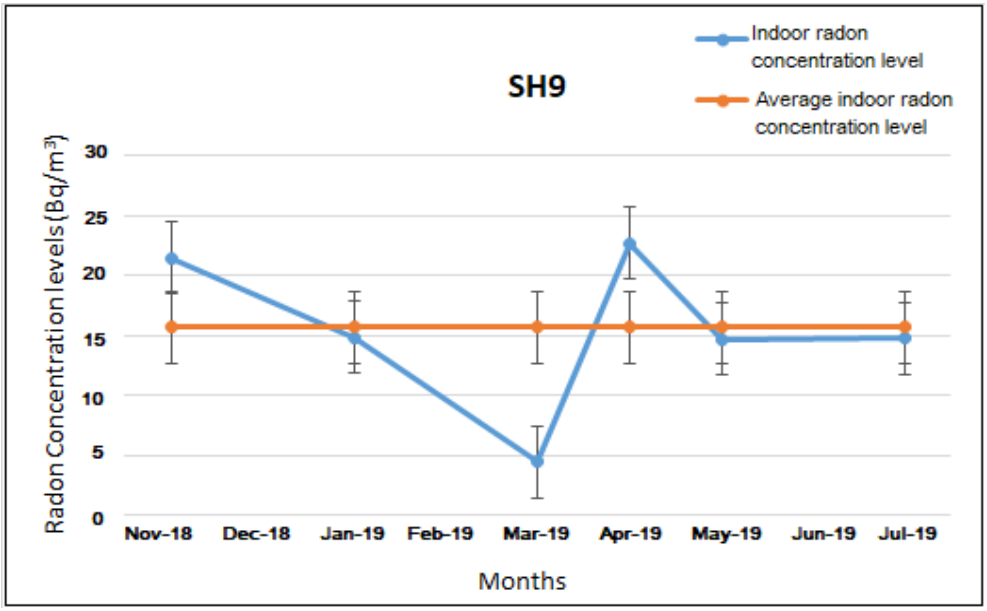


Figure 4.10: The distribution of indoor radon concentration levels in SH9 across the months relative to the average indoor radon concentration level.

SH10 had a similar scenario as SH9, the only difference is that, the drop in the radon concentration was experienced in May, refer to Figure 4.11.

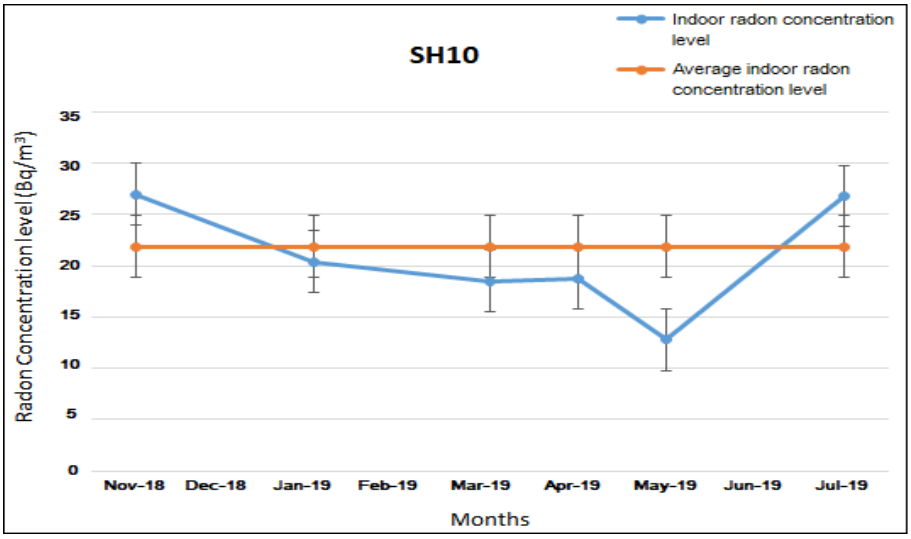


Figure 4.11: The distribution of indoor radon concentration levels in SH10 across the months relative to the average indoor radon concentration level.

PH1 (Figure 4.12) recorded relatively low radon concentrations throughout the months, with a high of 14.9 Bq/m^3 and an average of 6.8 Bq/m^3.

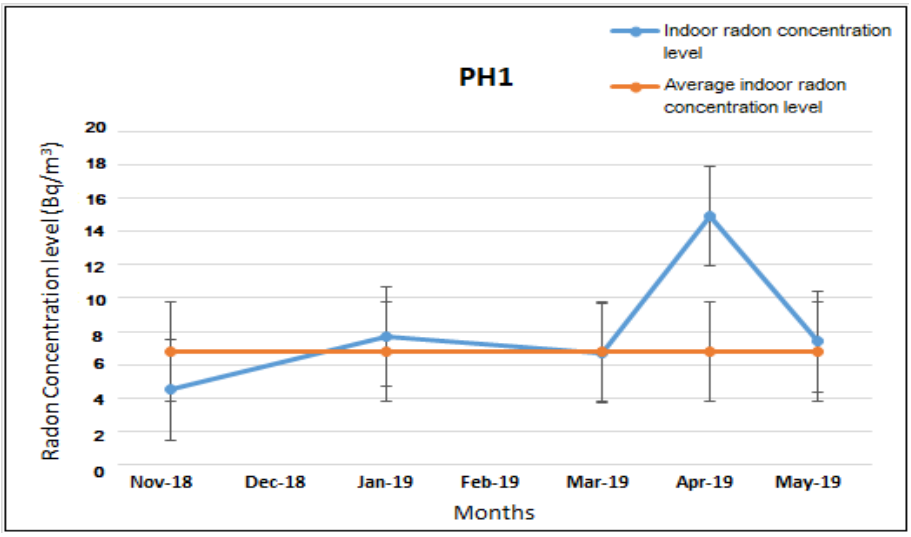


Figure 4.12: The distribution of indoor radon concentration levels in PH1 across the months relative to the average indoor radon concentration level.

There were some fluctuations in the radon concentration in PH2, nonetheless the overlaps

between the average and the true values indicated that PH2 generally experienced low concentrations of about 7.16 Bq/m^3 on average.

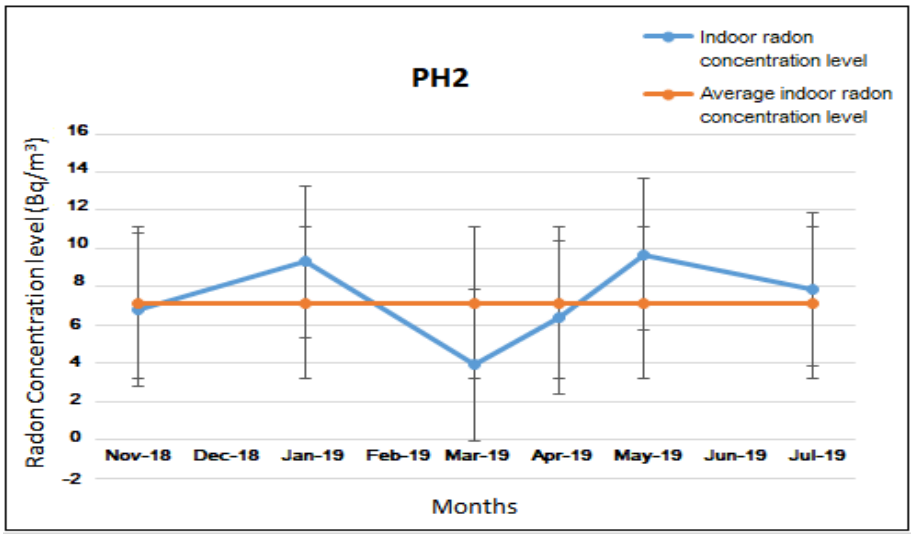


Figure 4.13: Distribution of indoor radon concentration levels in PH2 across the months relative to the average indoor radon concentration level.

In general, selected houses in Serule (mining area) show relatively high radon concentration levels compared to those in Palapye (non-mining area) on a month to month comparison.

4.2.2 Seasonal Variations

Indoor radon concentrations differ from season to season mainly because of meteorological parameters and pressure differences between the ground beneath and the pressure inside the house. There were some inconsistencies in the data collection due to unavailability of the residents during some data collection dates. Therefore, two of the houses (SH3 and SH4) where measurement wasn't acquired in one or two of the months were omitted for presentation purposes, see Figure 4.14, refer also to Appendix B for more details on SH3 and SH4. The measurement period spanned through three seasons, that is, summer (months, November to January), autumn (months, February to April) and winter (months, May to July).

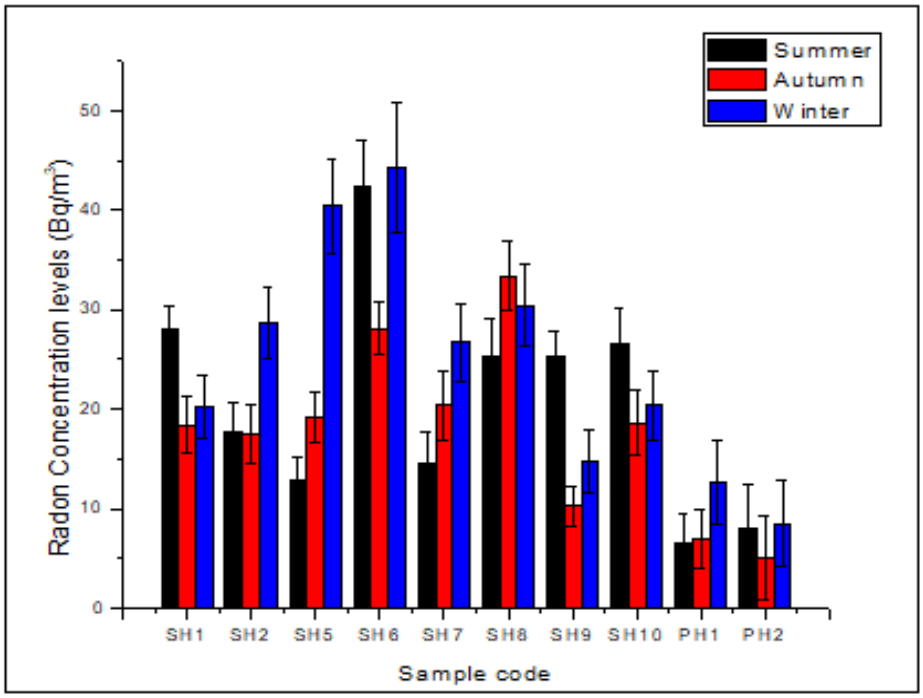


Figure 4.14: Seasonal variations of the radon concentration in the selected dwellings.

The highest concentration recorded was about 40 Bq/m^3 for winter (SH5 and SH6) and summer (SH6) seasons. SH1 recorded the highest concentration in summer with a value of 28.1 $\pm$ 2.3 Bq/m^3, SH2 and SH5 recorded the highest concentrations in winter, see Figure 4.14. SH6 recorded the highest concentrations in both summer and winter, SH9 had the highest concentration in summer and SH7 had relatively the same concentration across all the seasons. SH8, SH10, PH1 and PH2 recorded similar concentrations for all the 3 seasons as the values were within the uncertainties. Looking closely at Figure 4.14, it can also be observed that, slightly higher indoor radon concentration levels were recorded in summer than in autumn in most of the dwellings. Sample House 6 (SH6), had the highest radon concentration in summer at around 42.4 $\pm$ 4.6 Bq/m^3 and Sample House 8 (SH8) had the highest concentration in autumn at 33.4 $\pm$ 3.4 Bq/m^3. Indoor radon concentration levels experience temporal variations, meaning the concentration is not constant but varies with time, and this could be due to meteorological parameters

such as temperature, air pressure, precipitation and wind direction/speed which change from time to time.

It is important to note that, houses from SH1 to SH6 are located within the A-cap Resources uranium mining area. This could explain why these houses have relatively higher radon concentration levels as the underlying rocks may be rich in uranium. Ventilation habits of inhabitants could be another reason for elevated levels because ventilation is usually poor during winter and therefore, radon can accumulate in a house causing the levels to go up.

4.2.3 Influence of house design on the radon concentration

The design of the house along with the building materials used influences the indoor radon concentration level of a dwelling. Houses with cement floors (SH3, SH4, SH5 and SH6) recorded slightly higher radon concentrations compared to tiled houses (SH7, SH8, SH9, PH1 and PH2). House SH6 experienced relatively higher radon concentrations across the seasons mainly because of its design, refer to Table 3.1 on the building materials used for the construction of the houses on Chapter 3, section 3.2.2. It is important to note that SH6 was made of an iron shed which was poorly ventilated, making it easy for radon to accumulate in the dwelling.

House SH2 was made out of mud from the soil around the mining area and had an average indoor radon concentration of 20.9 ± 2.8 Bq/m^3. The house was however, well ventilated making radon to easily escape into the atmosphere, therefore an estimate could not be made of how much radon gets emanated from the mud wall.

4.3 Annual effective dose from inhalation of radon

The annual effective dose was calculated from an expression derived from UNSCEAR as already discussed in section 2.11 of Chapter 2. Table 4.2 shows the annual effective dose from inhalation of radon in each of the 12 sampled houses. The highest annual effective

dose obtained was 1.13 mSv from SH4 and the lowest was 0.17 mSv from PH1. The mean average annual effective dose received by the residents in the ten sampled houses in Serule was 0.67 ± 0.23 mSv, while in the control houses it was calculated to be 0.1764 ± 0.0071 mSv.

Table 4.2: The annual effective dose in the 12 sample houses.

Sample location	Annual effective dose (mSv)
SH1	0.56
SH2	0.53
SH3	0.66
SH4	1.13
SH5	0.76
SH6	1.00
SH7	0.51
SH8	0.61
SH9	0.40
SH10	0.55
PH1	0.17
PH2	0.18

The results obtained in the current work for the annual effective dose in each dwelling are well below the set dose limit of 3 - 10 mSv as per the ICRP recommendations [31]. It can be noted that houses or residents in Serule experience slightly higher annual effective doses as compared to the control houses in Palapye. It can further be observed that most houses within the mining area show higher annual effective doses than those outside the mining area in Serule.

4.4 Activity concentrations of ^{238}U, ^{232}Th and ^{40}K in the soil samples

The results of calculated activity concentrations of ^{238}U (series), ^{232}Th (series) and ^{40}K in soil samples collected from the selected houses are presented in Table 4.3. For the activity

concentration of ^{238}U series, the daughter radionuclide, ^{226}Ra was used to represent the series. ^{226}Ra is a gamma-ray emitting radionuclide in the ^{238}U decay series (see Figure 2.5), which subsequently decay to radon, ^{222}Rn. The average activity concentration of ^{232}Th was calculated from its identified daughter nuclides, that is ^{212}Pb and ^{228}Ac. See Appendix C for the calculated activity concentrations from different daughter nuclides.

Table 4.3: The activity concentrations of ^{226}Ra, ^{232}Th and ^{40}K.

Sample location	**^{226}Ra (Bq.kg^{-1})**	**^{232}Th (Bq.kg^{-1})**	**^{40}K (Bq.kg^{-1})**
SSH1	63.8 ± 18.9	25.3 ± 4.1	244.4 ± 20.0
SSH2	63.3 ± 19.6	19.6 ± 4.8	180.0 ± 19.6
SSH3	79.4 ± 23.1	44.1 ± 12.0	280.4 ± 26.2
SSH4	79.1 ± 25.3	36.9 ± 15.0	259.7 ± 23.3
SSH5	57.5 ± 20.3	8.3 ± 8.1	283.1 ± 25.8
SSH6	61.0 ± 20.8	26.4 ± 10.4	215.9 ± 22.6
SSH7	23.2 ± 15.6	36.2 ± 3.9	335.6 ± 28.2
SSH8	37.4 ± 17.1	24.9 ± 6.5	497.2 ± 34.6
SSH9	27.4 ± 14.9	28.3 ± 5.4	534.5 ± 36.4
SSH10	33.8 ± 17.0	31.6 ± 7.4	617.8 ± 40.9
SSH11	10.5 ± 15.1	-1.1 ± 7.3	220.3 ± 19.4
SSH12	28.0 ± 18.9	18.4 ± 5.4	324.2 ± 25.2
World Average Values ([5])	**35**	**30**	**400**

Higher levels of ^{238}U were found in areas within the mining area compared to those in the control areas, with the highest concentration being 79.4 ± 23.1 Bq.kg^{-1} from SSH3. From Table 4.3, the calculated ^{226}Ra activity concentration from SSH11 and the ^{232}Th activity concentrations from SSH5 and SSH11 were inconclusive since the calculated values were relative to uncertainties. Figure 4.15 illustrates the relative distribution of activity concentrations of ^{226}Ra from the soil samples collected and counted.

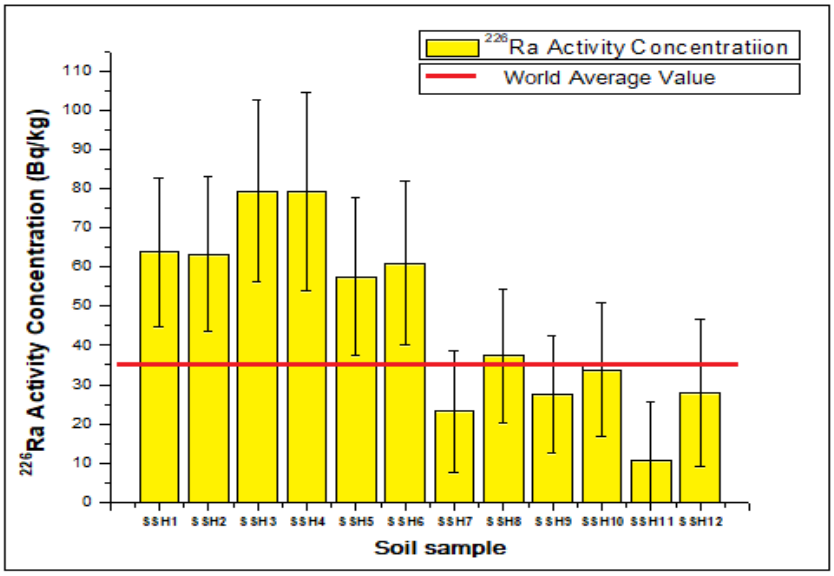


Figure 4.15: The ^{226}Ra activity concentration levels in the selected sampled locations.

There is a correlation between the radon concentration levels results and the activity concentration results, as houses with lower radon concentration levels also have lower ^{226}Ra activity concentrations levels. These houses are found outside the mining area. Houses with higher radon and ^{226}Ra activity concentrations are within the mining area in Serule.

The activity concentration of ^{232}Th in the soil samples was generally low with most concentrations being less than or equal to the world average value of 30 Bq.kg^{-1} [5]. The highest ^{232}Th activity concentration was found in SSH3 with a value of 44.1 ± 3.8 Bq.kg^{-1}, see Figure 4.16. Areas outside the mining area showed higher activity concentrations of ^{40}K compared to those within the mining area. SSH8, SSH9 and SSH10 had concentrations greater than the world mean average of 400 Bq.kg^{-1} [5], see Table 4.3 and also Figure 4.17. The reason for this, may be the use of potassium rich fertilizers by residents for agricultural production in their homes.

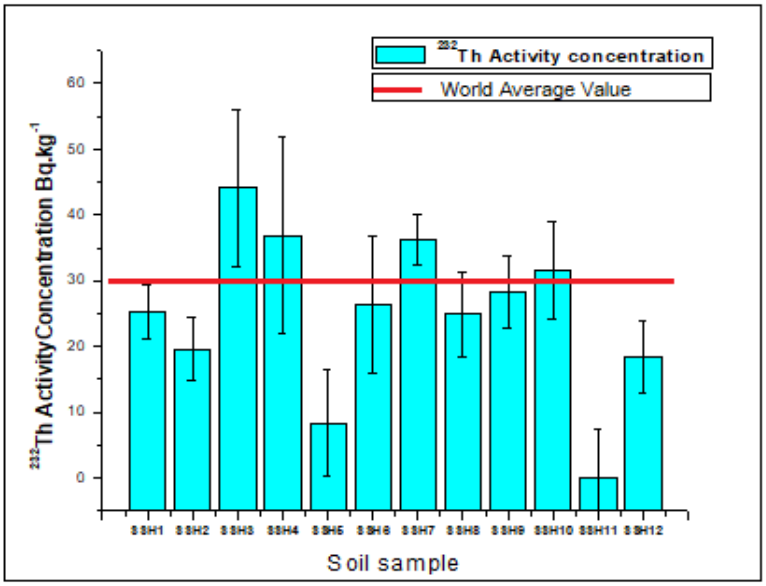


Figure 4.16: The ^{232}Th activity concentration levels in the selected sampled locations.

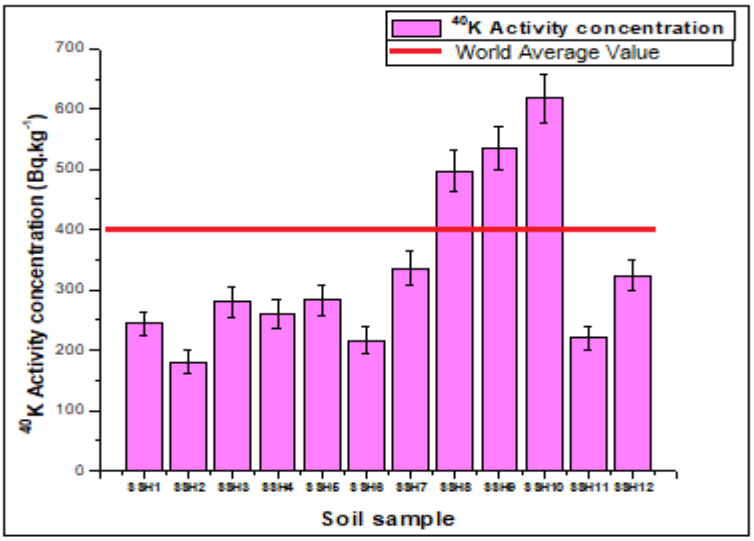


Figure 4.17: The ^{40}K activity concentration levels in the selected sampled locations.

4.4.1 Radiological hazard assessment for soil samples

The radiological hazard assessment of the soil samples were calculated using equations 3.7, 3.8, 3.9 and 3.10 in subsection 3.6.3 to determine the radium equivalent, absorbed dose, external and internal hazard indices. Table 4.4 shows the results of the calculated values. From the results, it can be observed that the highest Ra_{eq} calculated was from SSH3 with a value of 164.1 ± 12.2 Bq.kg^{-1}.

Areas within the mining area show slightly higher values of Ra_{eq} as compared to those outside the mining area. The results obtained for Ra_{eq} are well below the worldwide value of 370 Bq.kg^{-1} as recommended by the IAEA under normal conditions, see Figure 4.18.

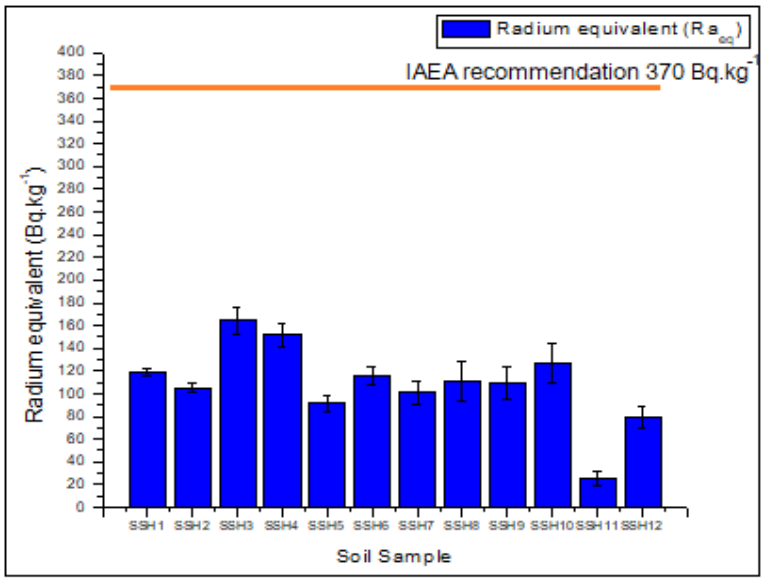


Figure 4.18: The Radium equivalent (Ra_{eq}) values for each soil sample.

Table 4.4: The calculated results of absorbed dose (D), radium equivalent (Ra_{eq}), external hazard index (H_{ex}) and internal hazard index (H_{in}).

Sample location	D ($nGy.h^{-1}$)	Ra_{eq} ($Bq.kg^{-1}$)	H_{ex}	H_{in}
SSH1	54.9 ± 3.3	118.8 ± 3.3	0.3	0.5
SSH2	48.4 ± 4.0	104.7 ± 4.0	0.3	0.5
SSH3	75.0 ± 12.2	164.1 ± 12.2	0.4	0.7
SSH4	69.6 ± 10.4	151.8 ± 10.5	0.4	0.6
SSH5	43.4 ± 7.8	91.2 ± 7.8	0.2	0.4
SSH6	53.1 ± 8.3	115.4 ± 8.3	0.3	0.5
SSH7	46.6 ± 10.2	100.8 ± 10.1	0.3	0.3
SSH8	53.0 ± 17.1	111.3 ± 17.1	0.3	0.4
SSH9	52.0 ± 14.6	109.0 ± 14.6	0.3	0.4
SSH10	60.4 ± 17.6	126.5 ± 17.6	0.3	0.4
SSH11	13.3 ± 6.2	25.8 ± 6.2	0.1	0.1
SSH12	37.5 ± 9.8	79.2 ± 9.8	0.2	0.3

The highest absorbed dose calculated was from SSH3 with a value of 75.0 ± 12.2 $nGy.h^{-1}$ followed by 69.6 ± 10.4 $nGy.h^{-1}$, see Table 4.4. These values are higher than the world average absorbed dose rate of 57 $nGy.h^{-1}$ [5], but the high values obtained do not pose any danger as they are less than the recommended level of 80 $nGy.h^{-1}$ [46]. The H_{ex} and H_{in} are also higher in SSH3 and SSH4 as compared to other sampled areas. The external and internal hazard indices are however lower than the set limit of 1.

4.5 Concentration of Heavy metals in soil samples

The results for the concentration (mg/kg) of heavy metals in the selected soil samples determined using ICP-MS are presented in Table 4.5 and also in Figure 4.19. The concentrations of only nine heavy metals are presented in Table 4.5 that is, chromium (Cr), nickel (Ni), arsenic (As), copper (Cu), zinc (Zn), cobalt (Co), mercury (Hg), lead (Pb) and cadmium (Cd). More details on the ICP-MS measurements can be found in Appendix D. BDL stands for below detection limit and n.a means non-applicable.

Table 4.5: The concentration of Heavy metals in the selected soil samples in mg/kg.

Sample location	Cr	Ni	As	Zn	Cu	Co	Pb	Hg	Cd
SSH4	54.620	35.952	13.822	53.798	30.595	15.995	17.381	0.021	0.045
SSH6	46.489	23.794	8.110	38.905	23.186	6.020	15.079	0.015	0.037
SSH7	158.213	98.267	3.462	109.282	49.351	27.420	10.880	0.009	0.100
SSH9	48.176	15.651	2.289	19.677	13.437	8.334	7.519	0.007	0.034
SSH12	51.572	12.548	1.750	23.236	7.486	4.407	5.486	BDL	0.013
WHO/FAO guidelines	**100**	**50**	**20**	**350**	**100**	**50**	**100**	**n.a**	**3**

It can be observed in Table 4.5 that SSH7 had the highest concentration of heavy metals. The chromium and nickel concentrations from SSH7 were much higher than the maximum allowable limit according to the WHO/FAO guidelines, with values of 158.213 mg/kg and 109.282 mg/kg respectively [45]. It is important to note that, SSH7 sample was from Serule but outside the mining area. Samples in Serule, that is SSH4, SSH6 and SSH9 generally show slightly higher heavy metals concentrations in comparison with SSH12 which was the control. The results obtained relate with the common trend from all other acquired results, that higher radiation concentrations are found in Serule area than the control areas.

Figure 4.19 represents the ratio of the concentration of heavy metals in the selected soil samples with respect to the concentration of heavy metals as per the WHO/FAO guidelines (SSH/WHO). Elements which are above 1, are above the WHO/FAO guidelines and as such an indicator of heavy metal pollution.

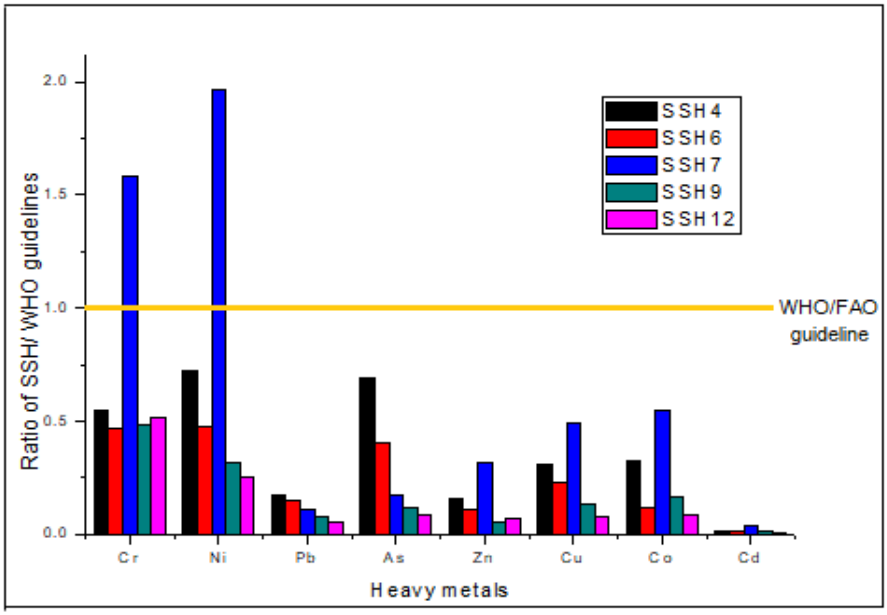


Figure 4.19: The ratio of heavy metals in selected soil samples with respect to WHO/FAO guidelines.

5

Conclusions and Recommendations

5.1 Introduction

This chapter gives a summary of the main findings of this study and also some recommendations.

5.2 Summary and conclusions

The main aim of this study was to determine the average indoor radon concentration level in residential houses in Serule area. The study also sought to determine the influence of seasonal variations and building materials on the radon concentration, the annual effective dose received by residents due to inhalation of radon gas, the activity concentration of some radionuclides in the sampled areas, the radiological hazard assessment and also to determine the concentration of heavy metals in the soil samples from the sampled areas.

The weighted average concentration of indoor radon in the ten sampled Serule houses was found to be 23.4 $\pm$ 2.1 Bq/m^3 measured using E-PERMS. Looking at individual sampled houses, houses SH4 and SH6 had the highest average indoor radon concentration of 44.8 $\pm$ 4.6 Bq/m^3 and 40.0 $\pm$ 7.2 Bq/m^3 respectively. Note that, houses SH4 and SH6 were within the mining area in Serule. Other sampled houses in Serule which were outside

the mining area had slightly lower radon concentrations compared to those that were within the mining area. The control houses in Palapye (PH1 and PH2) had an average radon concentration of 7.0 ± 0.3 Bq/m^3. It can therefore be concluded that, higher radon concentration levels are found in Serule because of the uranium rich underlying rocks. It is important to note that, even though the levels were higher in Serule, the overall indoor radon concentration levels obtained in this study were far below the set limit of 300 Bq/m^3 as recommended by the IAEA [4].

The indoor radon concentration level experiences temporal variations meaning, the concentration is affected by seasons. The results obtained indicated that the highest radon concentrations in almost all the twelve sampled houses were recorded in winter season than in summer and autumn. House SH6 had the highest concentration in winter and summer at about 44.3 ± 6.6 Bq/m^3 and 42.4 ± 4.6 Bq/m^3 respectively. The building material used in the construction of house SH6 attributed to such high concentrations because the iron shed was poorly ventilated, allowing for radon to easily accumulate inside the house. Houses SH1 to SH6 which were within the mining area showed higher concentrations across all seasons compared to those that were outside the mining area. It was also observed that houses with cement floors experienced slightly higher radon concentrations compared to those with tiled floors. Therefore, it can be concluded that seasonal variations along with building materials or house designs influence the radon concentration.

The average annual effective dose in Serule area from all the ten sampled houses due to inhalation of radon was calculated to be 0.67 ± 0.23 mSv. An average annual effective dose from the control area was found to be 0.1764 ± 0.0071 mSv. Residents of house SH4 received the highest annual effective dose of 1.13 mSv. The lowest dose received was from PH1 at about 0.17 mSv. The results of this study are well below the set dose limit of 3 - 10 mSv as per the recommendations by the ICRP [31].

The activity concentrations of ^{238}U, ^{232}Th and ^{40}K from the soil samples in the sampled areas were ranging from 6.0 - 658 Bq.kg^{-1}. The highest activity concentration levels of ^{238}U were found in areas within the mining area compared to those in the control areas.

The highest concentration was found to be 79.4 ± 23.1 Bq.kg^{-1} from the vicinity of house SH3 (SSH3). Activity concentrations of ^{232}Th were generally low with the highest value being 44.1 ± 3.8 Bq.kg^{-1} from SSH3. The results indicate that areas outside the mining area had higher activity concentrations of ^{40}K, with the highest value being 617.8 ± 40.9 Bq.kg^{-1}. The reason for this may be due to the use of potassium rich fertilizers by inhabitants for agricultural production in their homesteads.

The radiological hazard assessment was carried out in order to determine the radium equivalent (Ra_{eq}), absorbed dose, external (H_{ex}) and internal (H_{in}) hazard indices. The highest Ra_{eq} calculated was 164.1 ± 12.2 Bq.kg^{-1} from SSH3. It was observed that areas within the mining area had slightly higher Ra_{eq} values compared to those outside the mining area. The results obtained however, are below the worldwide value of 370 Bq.kg^{-1} as per the IAEA recommendations. The highest absorbed dose rate calculated was 75.0 ± 12.5 nGy.h^{-1} from SSH3 followed by 69.6 ± 10.4 nGy.h^{-1} form SSH4. These values were higher than the world average absorbed dose rate of 57 nGy.h^{-1}. The calculated values of H_{ex} and H_{in} for all the 12 sampled areas were below the set limit of 1, with the highest value being 0.7 from SSH3. These results are a further indication that uranium rich underlying rocks contribute to higher radiation levels.

The concentration of heavy metals in soil samples were determined using ICP-MS. Only nine heavy metals which have carcinogenic effects were considered in this study, that is chromium (Cr), nickel (Ni), arsenic (As), zinc (Zn), copper (Cu), cobalt (Co), lead (Pb), mercury (Hg) and cadmium (Cd). The results show that soil sample SSH7 from house SH7 in Serule area, had the highest concentration of heavy metals, with the Cr and Ni concentrations being higher than the maximum allowable limit of 100 mg/kg and 50 mg/kg with values of 158.213 mg/kg and 109.282 mg/kg respectively [45]. Soil samples in Serule area showed slightly higher heavy metal concentration in comparison to the control area.

In a nutshell, it can be concluded that the sampled areas in Serule experienced slightly low indoor radon concentration levels. However, the activity concentration of some radionuclides of ^{238}U, ^{232}Th and ^{40}K and higher absorbed dose rate values in some areas

in Serule are an indication that once mining starts, the radon from underground may easily seep out into the atmosphere or houses and contribute to higher concentrations. It is important to note that, the data recorded was not a representative of Serule but an indication of the need to carry out large scale surveys. The current study was limited to only ten houses due to the limited number of E-PERMS and the time available. A bigger sample size with few E-PERMS would have required a longer counting period which could not be afforded.

5.3 Recommendations

This study was carried out as a pilot investigation that could possibly lead to follow-up investigations especially once uranium mining starts in Serule. Only ten houses in Serule were used and two in Palapye as the control but as a recommendation for future research, large scale surveys should be carried out to get a more ideal representation of Serule area as a whole, maybe 100 or 200 sampling houses be used. The indoor radon concentration levels were measured using one set of equipment which are passive radon monitors called E-PERMS. It would be ideal to couple this set of equipment with an active radon monitor such as an AlphaGuard or RAD7 in order to get real-time radon concentration and for comparison purposes. The measurement period of radon concentration levels in this study spanned for roughly nine months but it would be ideal to measure the concentrations for an entire year. One other recommendation is, to measure meteorological parameters such as temperature and atmospheric pressure along with the radon concentration to see if the changes in those parameters affect the radon concentrations. A physics model that can be used to estimate the indoor radon concentration levels should be developed that encompasses all the other contributing factors such as building materials, activity concentration of underlying rocks, meteorological parameters, soil moisture, porosity and grain size.

Appendix A

Sampled houses dimensions

Table A.1: The dimensions of the rooms used in the current study, where the E-PERMS were deployed

Location	**Room dimensions (cm)**	**Height of E-PERM from the floor (cm)**	**GPS Coordinates**
SH1	510×470×275	160	S 21.88877° E 27.28854°
SH2	260×300×210	170	S 21.88877° E 27.28854°
SH3	350×380×205	160	S 21.88877° E 27.28854°
SH4	475×355×285	200	S 21.88877° E 27.28854°
SH5	320×320×220	160	S 21.88877° E 27.28854°
SH6	390×290×230	195	S 21.88877° E 27.28854°
SH7	550×420×270	190	S 21.88877° E 27.28854°
SH8	430×360×260	190	S 21.88877° E 27.28854°
SH9	380×370×260	220	S 21.88877° E 27.28854°
SH10	330×325×220	205	S 21.88877° E 27.28854°

Appendix B

Parameters for radon concentration calculation

The indoor radon concentration level when using E-PERMs is calculated using equation B.1 [37].

$$C_{Rn} = \frac{\Delta V}{C_f \times t} - BG, \tag{B.1}$$

where, C_{Rn} is the radon concentration in Bq/m^3, ΔV is the change in voltage (Initial voltage - Final voltage) in V, C_f is the calibration factor in units V per Bqm^{-3} d. The calibration factor for long term (LT) E-PERMS is given by

$$C_f(LT) = 0.0000168 \times \frac{V_i + V_f}{2} + 0.00481 \tag{B.2}$$

t is the time in days and BG is the environmental background radiation.

The electret voltages for every the measurement date were recorded in the sheet below. The calibration factor used to calculate the radon concentration can also be seen in the same sheet.

Data sheet for electret voltages, calibration factor and background radiation

Electret #	Sample Location	Background radiation (µSv/hr)	Initial Voltage (V) (15/10/2018)	Voltage read1 (V) (20/11/2018)	Voltage read2 (V) (16/01/2019)	Voltage read3 (V) (05/03/2019)	Voltage read4 (V) (16/04/2019)	Voltage read5 (V) (22/05/2019)	Voltage read6 (V) (03/07/2019)	Calibration factor (V/Bqm^{-3}.d
LW7262	SH1	0.029	770	746	710	686	668	653	634	0.01660
LW7264			781	762	493	477	461	449	432	0.01499
LW7290	SH2	0.035	780	767	738	717	702	679	651	0.01683
LW7292			771	755	719	692	669	655	621	0.01650
LW7267	SH3	0.052	774	753	722	692	-	634	599	0.01634
LW7268			772	744	712	680	-	619	583	0.01619
LW7283	SH4	0.042	774	739	-	624	585	-	510	0.01559
LW7285			776	749	-	668	636	-	560	0.01603
LW7270	SH5	0.049	774	746	527	500	-	-	-	
LW7272			771	751	725	700	673	640	604	0.01131
LW7405						764	730	697	659	0.01676
LW7277	SH6	0.041	760	712	657	625	420	389	348	0.01411
LW7282			778	750	706	674	646	615	581	0.01622
LW7457							771	730	691	0.01709
LW7314	SH7	0.045	778	-	730	699	675	-	625	0.01659
LW7340			772	-	726	701	677	-	626	0.01655
LW7341	SH8	0.046	777	757	731	-	684	654	624	0.01657
LW7345			771	735	689	-	638	623	589	0.01623
LW7295	SH9	0.041	691	659	634	621	602	586	569	0.01539
LW7297			774	752	367	22	-	-	-	
LW7389						765	744	728	708	0.01718
LW7304	SH10	0.042	790	764	737	711	691	679	647	0.01688
LW7305			775	738	699	674	650	632	611	0.01645
LW7357	PH1	0.075	767	749	718	697	672	654	378	0.01674
LW7358			774	730	679	652	625	414	370	0.014419
				Voltage 1 (V) (07/12/2018)	**Voltage 2 (V) (17/01/2019)**	**Voltage 3 (V) (06/03/2019)**	**Voltage 4 (V) (17/04/2019)**	**Voltage 5 (V) (22/05/2019)**	**Voltage 6 (V) (23/07/2019)**	
LW7366	PH2	0.075	771	752	732	711	691	672	642	0.01667
LW7375			769	748	721	697	675	656	624	0.016511

The uncertainty in the radon concentration is calculated using the sources of error associated with using E-PERMS [37].

E1. Error component No.1 related to the chamber volume, electret thickness and other chamber parameters and it is given by:

$$E1 = \pm 0.05 \times \frac{V_i - V_f}{CF \times t} \tag{B.3}$$

Where V_i is the initial voltage, V_f is the final voltage, CF is the calibration factor and t is the deployment period in days.

E2. Error component No. 2, related to the reading of electrets. It is given by:

$$E2 = \pm \frac{\sqrt{2}}{CF \times t} \tag{B.4}$$

E3. Error component No. 3, related to the uncertainty of natural background gamma radiation, and it is given by:

$$E3 = \pm (0.10 \times BG) \tag{B.5}$$

where BG is the background radiation in Bq/m^3.

ET. Error Total, is the overall error due to combining all the three errors associated with using E-PERMs. ET is given by:

$$E4 = \sqrt{E1^2 + E2^2 + E3^2} \tag{B.6}$$

Table B.1 shows the average radon concentration levels calculated in various seasons and the average concentration calculated for the entire measurement period. The dashes indicate that measurement was not carried out due to unavailability of residents during data collection days.

Table B.1: The average indoor radon concentration level in each dwelling in various seasons

Sample location code	Average indoor radon concentration in summer (Bq/m^3)	Average indoor radon concentration in autumn (Bq/m^3)	Average indoor radon concentration in winter (Bq/m^3)	Average indoor radon concentration in all three seasons (Bq/m^3)
SH1	28.1 ± 2.3	18.4 ± 2.8	20.2 ± 3.1	22.1 ± 1.9
SH2	17.8 ± 2.9	17.5 ± 2.9	28.7 ± 3.6	20.9 ± 2.8
SH3	18.1 ± 3.6	-	-	26.2 ± 3.9
SH4	-	-	53.7 ± 5.4	44.8 ± 4.6
SH5	12.8 ± 2.3	19.2 ± 2.5	40.4 ± 4.8	29.9 ± 4.0
SH6	42.4 ± 4.6	28.1 ± 2.6	44.3 ± 6.6	40.0 ± 7.2
SH7	14.6 ± 3.1	20.4 ± 3.5	26.7 ± 3.9	20.2 ± 3.2
SH8	25.3 ± 3.8	33.4 ± 3.4	30.4 ± 4.1	24.4 ± 3.5
SH9	25.3 ± 2.5	10.3 ± 2.0	14.7 ± 3.2	15.7 ± 2.9
SH10	26.5 ± 3.7	18.6 ± 3.3	20.4 ± 3.5	21.9 ± 3.2
PH1	6.5 ± 2.9	7.0 ± 3.0	12.7 ± 4.2	6.8 ± 2.9
PH2	8.1 ± 4.3	5.0 ± 4.2	8.5 ± 4.3	7.2 ± 4.1

Appendix C

Activity Concentration of observed radionuclides

The activity concentration was calculated using the equation C.1.

$$A = \frac{N}{\varepsilon_f \times I \times m \times t_s} \tag{C.1}$$

The uncertainty of the activity concentrations was calculated using propagation of errors. That is,

$$\delta A = A \times \sqrt{(\frac{\delta N}{N})^2 + (\frac{\delta \varepsilon_f}{\varepsilon_f})^2}, \tag{C.2}$$

where A is the activity concentration and δA is the uncertainty in activity concentration, N is the true counts and δN is the uncertainty in the true counts and ε_f is the efficiency of the detector and $\delta\varepsilon_f$ is the uncertainty in the efficiency.

Tables C.1 and C.2 show the observed radionuclides from the ^{238}U and ^{232}Th decay chains.

Table C.1: The activity concentrations of observed ^{238}U daughter radionuclides.

Sample location	^{226}**Ra** (**Bq.kg**$^{-1}$)	^{214}**Pb** (**Bq.kg**$^{-1}$)	^{214}**Bi** (**Bq.kg**$^{-1}$)
SSH1	63.8 ± 18.9	36.7 ± 6.6	32.3 ± 16.7
SSH2	63.3 ± 19.6	26.9 ± 4.3	22.5 ± 15.4
SSH3	79.4 ± 23.1	69.0 ± 11.7	55.5 ± 30.7
SSH4	79.1 ± 25.3	56.0 ± 4.3	21.9 ± 18.4
SSH5	57.5 ± 20.3	43.5 ± 3.7	14.8 ± 16.1
SSH6	61.0 ± 20.8	57.3 ± 10.2	50.0 ± 46.8
SSH7	23.2 ± 15.6	39.2 ± 1.6	21.6 ± 27.8
SSH8	37.4 ± 17.1	35.1 ± 1.9	40.6 ± 19.5
SSH9	27.4 ± 14.9	32.3 ± 6.7	18.8 ± 14.1
SSH10	33.8 ± 17.0	25.1 ± 5.1	42.3 ± 22.2
SSH11	10.5 ± 15.1	1.2 ± 2.5	4.2 ± 8.0
SSH12	28.0 ± 18.9	10.0 ± 4.5	5.8 ± 15.5

Table C.2: The activity concentrations of observed ^{232}Th daughter radionuclides.

Sample location	^{212}**Pb** (**Bq.kg**$^{-1}$)	^{212}**Bi** (**Bq.kg**$^{-1}$)	^{228}**Ac** (**Bq.kg**$^{-1}$)	^{208}**Tl** (**Bq.kg**$^{-1}$)
SSH1	11.6 ± 3.2	47.9 ± 12.5	39.1 ± 11.4	34.4 ± 0.3
SSH2	6.9 ± 2.8	43.7 ± 13.9	32.3 ± 12.4	28.8 ± 10.7
SSH3	40.4 ± 4.5	46.1 ± 16.3	47.9 ± 28.6	39.5 ± 17.1
SSH4	30.7 ± 4.4	49.7 ± 18.4	43.1 ± 34.4	30.6 ± 15.5
SSH5	-2.1 ± -3.3	10.8 ± 14.1	18.7 ± 12.9	18.5 ± 4.5
SSH6	18.9 ± 4.0	54.7 ± 15.3	33.9 ± 24.9	28.4 ± 18.9
SSH7	28.2 ± 4.3	42.7 ± 11.9	44.2 ± 12.1	35.1 ± 9.5
SSH8	25.3 ± 3.5	23.3 ± 12.6	24.5 ± 16.5	30.2 ± 13.0
SSH9	19.8 ± 3.4	46.1 ± 12.5	36.7 ± 14.3	31.7 ± 9.7
SSH10	38.2 ± 3.9	34.3 ± 14.2	24.9 ± 18.7	27.2 ± 23.3
SSH11	-8.30 ± -2.15	8.5 ± 3.9	6.04 ± 12.4	10.1 ± 9.0
SSH12	12.5 ± 3.3	4.3 ± 3.9	24.3 ± 14.1	22.6 ± 18.5

Appendix D

ICP-MS results from the Central Analytical Facilities (CAF)

ICP-MS was used in determining the concentration of heavy elements as already mentioned. The results obtained are of heavy elements found in the five soil samples that were measured. The elemental concentrations in the soil are given in units μg/kg but were converted to mg/kg in the current study.

ICP-MS Laboratory
CAF Central Analytical Facilities
STELLENBOSCH UNIVERSITY
Agilent Technologies
Authorized Partner Laboratory

	B ug/kg	V ug/kg	Cr ug/kg	Mn ug/kg	Co ug/kg	Ni ug/kg	Cu ug/kg	Zn ug/kg
LOD	**4098**	**3**	**91**	**59**	**3**	**31**	**235**	**53**
% Accuracy QC	**92**	**99**	**99**	**96**	**97**	**98**	**98**	**101**
% Recovery WQB-1	**111**	**108**	**107**	**92**	**100**	**99**	**100**	**97**
SSH4	11662	113594	54620	217995	15995	35952	30595	53798
SSH6	11669	52556	46489	179737	6020	23794	23186	38905
SSH 7	12225	93962	158213	572819	27422	98267	49351	109282
SSH 9	*BDL	40597	48176	279736	8334	15651	13437	19677
SSH 12	*BDL	23408	51575	112940	4407	12548	7486	23236

***BDL_Below Detection Limit**

	As ug/kg	Se ug/kg	Sr ug/kg	Mo ug/kg	Cd ug/kg	Sn ug/kg	Sb ug/kg	Ba ug/kg	Hg ug/kg
LOD	**69**	**12**	**7**	**5**	**0.0**	**13**	**3**	**2**	**5**
	101	**99**	**95**	**94**	**102**	**98**	**101**	**101**	**123**
	108	**85**	**118**	**115**	**96**	**113**	**97**	**119**	**90**
	13822	305	38856	494	45	1591	167	120988	21
	8110	181	25201	511	37	2188	94	87189	15
	3462	318	19393	437	100	1779	80	130021	9
	2289	302	7737	538	34	805	67	92952	7
	1750	98	4915	58	13	599	115	52533	*BDL

	Pb ug/kg	Al mg/kg	Fe mg/kg	Ca mg/kg	K mg/kg	Mg mg/kg	Na mg/kg	P mg/kg	Si mg/kg
LOD	**6**	**15**	**5**	**50**	**50**	**50**	**50**	**50**	**50**
	97	**106**	**104**	**100**	**99**	**100**	**97**	**103**	**101**
	97	**121**	**109**	**106**	**133**	**109**	**119**	**105**	
	17381	57686	15881	2158	3109	1490	187	218	1193
	15079	52057	17125	2525	3940	2031	148	176	1218
	10880	61782	60158	2115	5391	3592	227	289	1169
	7519	21922	22357	630	3882	2196	243	283	1189
	5486	14945	11178	2897	3556	1107	98	85	1873

References

[1] M. S. Karim, H. H. Daroysh, and A. N. Mohammed, "Assessment of Indoor Radon Concentrations in Dwellings for Baghdad Governorate by Using RAD-7 Detector," *Detection*, vol. 4, no. 02, p. 40, 2016.

[2] N. K. Ahmed and A. G. M. El-Arabi, "Natural radioactivity in farm soil and phosphate fertilizer and its environmental implications in Qena Governorate, Upper Egypt," *Journal of environmental radioactivity*, vol. 84, no. 1, pp. 51–64, 2005.

[3] R. O. Hussain and H. H. Hussain, "Natural occurring radionuclide materials," in *Radioisotopes-Applications in Physical Sciences*, IntechOpen, 2011.

[4] L. Gue, *Revisiting Canada's Radon Guideline*. David Suzuki Foundation, 2015.

[5] UNSCEAR, "Effects of ionizing radiation," *United Nations, New York*, pp. 453–487, 2000.

[6] F. Bou-Rabee, A. Z. Al-Zamel, R. A. Al-Fares, and H. Bem, "Technologically enhanced naturally occurring radioactive materials in the oil industry (TENORM).," *Nukleonika*, vol. 54, pp. 3–9, 2009.

[7] UNSCEAR, "United Nations Scientific Committee on the Effects of Atomic Radiation, Effects and Risks of Ionizing Radiation, Report to the General Assembly with Scientific Annexes, Volume 1.," United Nations, New York, 2006.

[8] P. Mishra, R. Rawat, V. Sharma, and A. Saxena, "Concentration of Radon and its Progeny Levels in Air in the Dwellings of Moradabad of Western UP," *India.(IJSR)*, vol. 5, no. 2, 2014.

[9] C. H. Clement, M. Tirmarche, J. Harrison, D. Laurier, F. Paquet, E. Blanchardon, and J. Marsh, "Lung cancer risk from radon and progeny and statement on radon," *Annals of the ICRP*, vol. 40, no. 1, pp. 1–64, 2010.

[10] C. Brough, R. Bowell, J. Grogan, J. Randabel, and P. Woolrich, "Letlhakane project: case study in complex uranium mineralogy and its geometallurgical implications," *Mining Technology*, vol. 122, no. 1, pp. 53–61, 2013.

[11] A. Allisy, "Henri Becquerel: the discovery of radioactivity," *Radiation protection dosimetry*, vol. 68, no. 1-2, pp. 3–10, 1996.

[12] T. Santawamaitre, P. Regan, D. Bradley, M. Matthews, D. Malain, and H. Al-Sulaiti, "An evaluation of the level of naturally occurring radioactive material in soil samples along the Chao Phraya river basin," *Nuclear Instruments and Methods in Physics Research Section A: Accelerators, Spectrometers, Detectors and Associated Equipment*, vol. 619, no. 1-3, pp. 453–456, 2010.

[13] V. Gruber, "Radiation exposure by natural radionuclides in drinking water in upper austria: a radioanalytical and hydrogeological research and evaluation in an international context," 2009.

[14] M. Ivanovich and R. S. Harmon, *Uranium series disequilibrium: applications to environmental problems*. Oxford University Press, USA, 1982.

[15] J. Peterson, M. MacDonell, L. Haroun, F. Monette, R. D. Hildebrand, and A. Taboas, "Radiological and chemical fact sheets to support health risk analyses for contaminated areas," *Argonne National Laboratory Environmental Science Division*, vol. 133, 2007.

[16] K. Krane, "Alpha decay," *Introductory Nuclear Physics*, pp. 246–271, 1988.

[17] IAEA, *National and Regional Surveys of Radon Concentration in Dwellings: Review of Methodology and Measurement Techniques*. IAEA, 2013.

[18] W. W. Nazaroff and A. V. Nero, "Radon and its decay products in indoor air," 1988.

[19] Y. Ishimori, K. Lange, P. Martin, Y. Mayya, and M. Phaneuf, *Measurement and calculation of radon releases from NORM residues*. IAEA, 2013.

[20] S. A. Durrani *et al.*, *Radon measurements by etched track detectors: applications in radiation protection, earth sciences and the environment*. World Scientific, 1997.

[21] C. E. Lawrence, *Measurement of 222Rn exhalation rates and 210Pb deposition rates in a tropical environment*. PhD thesis, Queensland University of Technology, 2006.

[22] F. J. Aldenkamp and P. Stoop, "Sources and transport of indoor radon," 1994.

[23] C. Edsfeldt, *The radium distribution in some Swedish soils and its effects on radon emanation*. PhD thesis, Institutionen för anläggning och miljö, 2001.

[24] J. Heritage, "Radon pinpointing a mystery," *EPA Journal*, vol. 12, no. 6, 1986.

[25] G. Swedgemark and L. Mjones, "Radon and radon daughter concentrations in Swedish homes," *Radiation protection dosimetry*, vol. 7, no. 1-4, pp. 341–345, 1984.

[26] Green and H. H. initiative, "Springfield healthy homes." https://springfieldhealthyhomes.org/radon/. Accessed November 11, 2019.

[27] S. Darby, D. Hill, A. Auvinen, J. Barros-Dios, H. Baysson, F. Bochicchio, H. Deo, R. Falk, F. Forastiere, M. Hakama, *et al.*, "Radon in homes and risk of lung cancer: collaborative analysis of individual data from 13 European case-control studies," *Bmj*, vol. 330, no. 7485, p. 223, 2005.

[28] WHO, *WHO handbook on indoor radon: a public health perspective*. World Health Organization, 2009.

[29] ICRP, "International commission on radiological protection publication 103," *Annals ICRP*, vol. 37, no. 2.4, p. 2, 2007.

[30] D. R. Fisher and F. H. Fahey, "Appropriate use of effective dose in radiation protection and risk assessment," *Health physics*, vol. 113, no. 2, p. 102, 2017.

[31] "Protection against Radon-222 at Home and at Work., author=ICRP," *ICRP Publication 65. Ann. ICRP*, vol. 23, 1993.

[32] R. Lindsay, R. Newman, and W. Speelman, "A study of airborne radon levels in Paarl houses, South Africa and associated source terms, using electret ion chambers and gamma-ray spectrometry," *Applied radiation and isotopes*, vol. 66, no. 11, pp. 1611–1614, 2008.

[33] C. E. Andersen, O. Raaschou-Nielsen, H. P. Andersen, M. Lind, P. Gravesen, B. L. Thomsen, and K. Ulbak, "Prediction of 222Rn in Danish dwellings using geology and house construction information from central databases," *Radiation protection dosimetry*, vol. 123, no. 1, pp. 83–94, 2007.

[34] O. Dikinya, "Heavy metals and radionuclide status and characterisation of pre-mined soils in Serule, North East Botswana," *Environmental earth sciences*, vol. 73, no. 9, pp. 5405–5413, 2015.

[35] S. Botswana, "Population of town, villages and associated localities," *Statistics Botswana, Gaborone*, 2011.

[36] G. Instruments, *AlphaGUARD portable radon monitors user manual*. Germany, 1998.

[37] P. Kotrappa, J. Dempsey, R. Ramsey, and L. Stieff, "A practical E-PERM TM (electret passive environmental radon monitor) system for indoor 222Rn measurement," *Health Physics*, vol. 58, no. 4, pp. 461–467, 1990.

[38] W. J. Speelman, *Modelling and measurement of radon diffusion through soil for application on mine tailings dam*. PhD thesis, University of the Western Cape, 2004.

[39] Automess, *Automess Automatik und Messtechnik GmbH, Operating Manual for the Dose Rate Meter 6150AD*. 2005.

[40] A. D. Joseph, *Radiometric study of soil: the systematic effects*. PhD thesis, University of the Western Cape, 2007.

[41] S. Harb, D. Salahel, A. Abbady, *et al.*, "Study of efficiency calibrations of HPGe detectors for radioactivity measurements of environmental samples," 2008.

[42] R. Newman, R. Lindsay, K. Maphoto, N. Mlwilo, A. Mohanty, D. Roux, R. De Meijer, and I. Hlatshwayo, "Determination of soil, sand and ore primordial radionuclide concentrations by full-spectrum analyses of high-purity germanium detector spectra," *Applied Radiation and Isotopes*, vol. 66, no. 6-7, pp. 855–859, 2008.

[43] C. Kamunda, M. Mathuthu, and M. Madhuku, "Health risk assessment of heavy metals in soils from witwatersrand gold mining basin, South Africa," *International journal of environmental research and public health*, vol. 13, no. 7, p. 663, 2016.

[44] M. Mohammad, M. Khali, and F. Khrais, "Measurement of activity concentration levels of radionuclides in soil samples collected from Bethlehem Province, West bank, Palestine," *Turk J Eng Environ Sci*, vol. 38, pp. 113–125, 2014.

[45] C. A. Commission *et al.*, "Food additives and contaminants, Joint FAO," *WHO food standards programme, ALINORM*, vol. 1, pp. 1–289, 2001.

[46] U. N. S. C. on the Effects of Atomic Radiation *et al.*, "Sources and effects of ionizing radiation: UNSCEAR 1993 report to the General Assembly," *New York, NY: United Nations*, pp. 280–283, 1993.